COMET

Project:

Chemical Looping for efficient biomass utilization

Project acronym:

BIO-LOOP

Second interim report

submitted to BEST – Bioenergy and Sustainable Technologies GmbH

Authors:

Dipl.-Ing. Benjamin **Fleiß**
Dipl.-Ing. Dr.techn. Josef **Fuchs**
Dipl.-Ing. Dr.techn. Stefan **Müller**
Univ.-Prof. Dipl.-Ing. Dr.techn. Hermann **Hofbauer**

Institute of Chemical, Environmental and Bioscience Engineering
TU Wien
Getreidemarkt 9/166
1060 Wien

Vienna, 25.03.2022

Content

1 Project 1: Deliverable 1.1

Based on chemical looping combustion (CLC) experiments in the laboratory unit, recommendations for material development of oxygen carrier (OC) were elaborated in Deliverable 1.1. The findings of Milestone 1.1 about characterization and assessment of OC were expanded. The important distinction between carrier specific and fluidized bed specific properties was adopted and applied to ten different OC. The assessment did not only show the advantage and weaknesses of different OC, but also indicated which properties should be of particular priority for material production. The assessment of the OC was supplemented by different extended analysis methods, which are given in the "Sub-report XRD" and "Sub-report SEM and BET", see Appendix. Furthermore, a methodology was designed how to further investigate important properties, which were not included in the assessment scheme. A detailed attrition rate, cycle stability and influence of ash layer could only be investigated in long-term experiments. These investigations were designed to represent experimental conditions close to reality of steady state operation of reactors of larger scale in regard to temperature, fuel to OC ratio and oxidation state. In a first step the reactivity of an OC with different oxidations states was tested. The preliminary results were used to recommend actions for material production and helped optimizing synthesis routes for development of successful OC.

1.1 Methodology laboratory experiments

1.1.1 Laboratory unit

Many CLC reactors published in literature use the dual fluidized bed (DFB) concept, ranging in scale from small sizes of about 1.5 kW_{th} up to 1 MW_{th} pilot plants. In contrast to the common DFB design, the laboratory unit of this work is designed as a simple fluidized bed to investigate both the oxidation and the reduction reaction independently from each other. The AR- and FR-operation can be simulated alternating transiently up to 1000 °C. With an inner diameter of 13 cm and a total height of about 1 m, the reactor uses a bubbling fluidized bed at about 10 cm height, shown in Figure 1. Half of the overall reactor height is designed as freeboard for preventing particle discharge. The desired operation temperature can be obtained by electrical heating of the fluidized bed using heating shells. Fuels can be added through a fuel pipe onto the fluidized bed. This on-bed feeding is realized by a nitrogen-flushed fuel lock to prevent air contamination and an igniting atmosphere. An important feature of the reactor is the in-situ bed material sampling system, which allows the extraction of bed material through a moveable basket during operation. A detailed description of the reactor can be found at Pachler (2019).

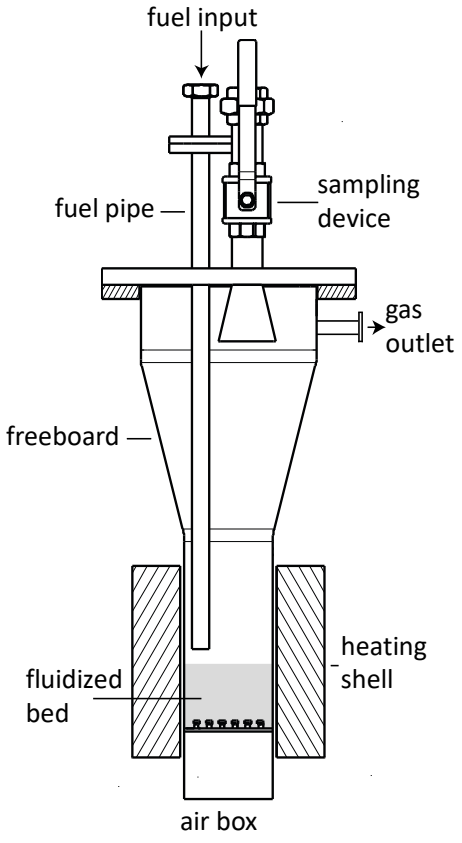

Figure 1: Layout of the reactor with a sampling device, different fuel pipes and heating shell. (values given in mm)

[1] The labortory unit can be operated with different gases from air, nitrogen and steam to methane and is designed as a fluidized bubbling bed. For experimental evaluation, the measuring equipment of the reactor consists of temperature, pressure and gas measurements. A five components measurement device records the concentrations of CO_2, CO, O_2, H_2 and CH_4. A slip stream of the exhaust gas is taken for this purpose, first cooled in a condenser, and further cleaned in RME (rape methyl ester) scrubbers. Further information is also published in Fleiß et al. (2021). [2]

1.1.2 Oxygen carriers and fuel

The different OC were used as a base for the comparison in experimental form. The elemental composition of some of the OC is given in Table 1. The natural ores, all have different composition, particle size and distribution. An advantage of some of the OC is the oxygen uncoupling ability (CLOU), which is a known effect for some manganese and copper containing OC. This allows the material to release oxygen without direct reaction with fuel based on the instability of metal oxide at certain temperatures and oxygen partials pressures. [3]

Table 1: The elemental composition of the three used OC

	Ilmenite	Braunite	Mn ore	Al Cu	Lana	Olivin	IOC ore
Al (wt%)	0.3	0.3	1.8	42.8	-	0.3	0.1
Ba (wt%)	-	0.2	-	-	-	-	-
Ca (wt%)	0.2	3.5	0.2	0.2	27.1	0.3	0.2
Cu (wt%)	-	-	-	8.5	-	-	-
Fe (wt%)	35.5	11.0	42.1	-	0.5	7.3	66.8
Mg (wt%)	2.8	0.9	0.3	-	2.3	30.2	0.2
Mn (wt%)	0.2	55.0	21.8	0.2	31.7	0.2	0.1
Na (wt%)	0.1	0.2	0.1	-	-	0.2	-
S (wt%)	0.2	0.1	-	-	0.1	0.1	-
Si (wt%)	1.1	2.5	2.9	0.2	0.1	19.6	2.142
Ti (wt%)	27.9	-	0.1	0.1	4.5	0.1	0.1
O (wt%)	Rest	Rest	Rest	Rest	Rest	Rest	Rest

OC materials must not only fulfil a number of different criteria in order to be suitable, the main additional cost for CLC is also their replacement, required due to attrition and deactivation. OC need to have sufficient oxygen transport capacity R_O, with high reactivity for both reduction and oxidation reactions, and both must be maintained over a large number of redox cycles. Moreover, OC need to have favorable thermodynamics with regard to fuel conversion to CO_2 and H_2O. In addition, good fluidization properties and no agglomeration tendencies in both reducing and oxidizing atmosphere are also fundamental for successful CLC operation. [4]

Softwood pellets of class EN-plus A1 according to ISO 17225-2 with a diameter of 6 mm and a length of 3-40 mm were used as fuel. These pellets are characterized by a low ash content and Sulphur/chlorine content, which is important for the experiments, because less interference based on ash and fuel contaminations occur. A detailed fuel analysis was made by the accredited and notified testing laboratory for combustion systems at TU Wien and can be found at Benedikt et al. (2017). [5]

1.1.3 Experimental evaluation

During the experiments solid samples of the OC at each operating point were extracted. The oxygen transport can be determined using a procedure developed by Kolbitsch et al. 2009. [6] After the experiments, a sieve analysis of the bed material was carried out and the loss of bed material was determined. In fact, the cyclone with included filters is emptied the first time, where the gas velocity is the highest. Most of the fine particle should be discharged during this experiment. After the last experimental point, the content of the cyclone is weighted and the resulted weight only comes from discharged particle abraded from the OC, because the amount of ash can be neglected due to the low ash content of the fuel. Based on Equation 1, an attrition rate of the OC, stressed by cyclic CLC operation, can be estimated via this weighed discharge. [7]

$$A_{tot} = \frac{m_{f,t}}{m} \cdot {t_{T2-F1}}^{-1} \cdot 100 \qquad [\text{wt\%/h}] \qquad (1)$$

The OC to fuel ratio φ gives information about the theoretical available oxygen during the experiments. Thus, it can be calculated using Equation 2. The calculation includes the oxygen transport capacity R_O of the whole reactor filling m of the OC and compares it with the stoichiometric oxygen demand of the fuel for complete combustion $m_{O2,st}$.

$$\phi = \frac{R_O \cdot m}{m_{O2,st}} \qquad [\text{kg/kg}] \qquad (2)$$

In addition, the concentration of the gases CO_2, CO, H_2 and CH_4 was measured to assess the performance of the OC in each experiment. Consequently, important performance parameters can be elaborated by calculating the total amount of the components. One key parameter is the carbon conversion rate X_C, with which the reaction of fuel to gas can be identified. [8] Equation 3 shows the carbon conversion rate, calculated by dividing the amount carbon found in the gas phase by the carbon contained in the fuel. The balance to 100% results from higher hydrocarbons, tars and coke.

$$X_C = \frac{n_{C,gas}}{n_{C,fuel}} \cdot 100 \qquad [\%] \qquad (3)$$

Another important parameter is the selectivity (S_n) of the different carbon containing gases. The selectivity is an indication of complete fuel combustion. Thus, the equation contains the total amount of carbon in the exhaust gas $n_{C,gas}$ and the carbon contained in the gas specie n ($n_{C,n}$). Equation 4 can be assembled for S_{CO2}, S_{CO} and S_{CH4}.

$$S_n = \frac{n_{C,n}}{n_{C,gas}} \cdot 100 \qquad [\%] \qquad (4)$$

A combination of the two previous performance parameters results in the yield (Y_n) of a certain gas, shown in Equation 5. It calculates the amount of carbon, converted to the gas, per fuel input of carbon.

$$Y_n = X_C \cdot S_n = \frac{n_{C,n}}{n_{C,fuel}} \cdot 100 \quad [\%] \quad (5)$$

1.1.4 Fluidized bed properties for assessment

Density of bed material particles:

In a DFB system, the density of the bed material particles determines largely the amount of OC that can be transported between the reactors. Higher density results therefore in a fluidized bed with closely spaced particles with given gas velocities and enables the transport of more mass of hot material for the same transported volume over the reactors. This reduces the temperature spread between the AR and the FR and provides sufficient heat transport for the combustion reaction. A low density can limit the solid circulation rate, thus impacting fuel conversion and lifetime, due to higher reduction of the particles, negatively. In addition, high density OC allow the FR to be operated with more steam without causing bed material discharge. This leads to a higher steam to carbon ratio and can thereby support the gasification reaction. [9] In the experiments with the laboratory unit, the density of the materials, in addition to the particle diameter, had a direct influence on the amount of steam that could be added in the reduction cycle to achieve the targeted experimental conditions. For the density measurement, the three materials, in a defined oxidized state (after heat treatment at 600 °C), were mixed with water in a defined volume, resulting in a density estimation in water.

Bulk density of bed material:

The bulk density of OC determines the filling quantity of reactors to reach certain filling heights and the available oxygen with given oxygen transport capacity. That means with higher bulk density more OC can be filled into the reactor and more oxygen for reaction is therefore available. The bulk density measurement of the OC was carried out according to DIN EN ISO 60. For the laboratory reactor, the bulk density at a fixed reactor filling height resulted therefore in the following filling quantities.

Particle size and particle size distribution:

Fluidized bed reactors are designed for specific bed materials with a certain particle size. Therefore, it is important that the particle size distribution does not deviate too much from the requirements of the plant. A narrower particle size distribution around the mean particle diameter can benefit operation, because the conditions in the reactor can be controlled more precisely. Especially the finest particles cause problems, because of discharging and reducing the total filling of the reactor. However, very coarse particles can also impair the mixing in a fluidized bed. [10] Of course, sieving to a narrower distribution can be carried out before being used in plants. However, each treatment step of OC is also accompanied with increased costs. The particle size and the distribution of the three OC was determined by sieve analyses. The particle size, similar to the density, influences the amount of steam needed to reach a certain fluidization point according to the Reh-diagram. [11] Particles sizes below 100 and above 400 µm were considered unsuitable for operation in the presented reactor system and their summed mass fraction was compared between the OC.

Attrition rate:

The attrition rate indicates the stability of the bed material during long-term operation. The abrasion of the particles is discharged as fine particles and reduces the total bed mass. Stable long-term operation is made considerably more difficult with a high attrition rates of the OC. In addition, the bed material needs to be replaced regularly and this increases the cost of operation. [12-14] Based on the particles discharged into the cyclone, an attrition rate was determined over the experimental time according to Equation 1. The attrition rate indicates the stability of the bed material during long-term operation. The abrasion of the particles is discharged as fine particles and reduces the total bed mass. Stable long-term operation is made considerably more difficult with a high attrition rates of the OC. In addition, the bed material needs to be replaced regularly and this increases the cost of operation. [12-14] The attrition rate obtained in this way serves as a comparative tool for the OC tested in the laboratory reactor. This is a simplified representation of the attrition rate due the fact that it is highly impacted by reduction state, temperature change and number of cycles. However, the comparison with literature shows that the obtained values are still meaningful and can function as a basic estimation tool. [35, 36]. Fine abrasion is discharged from the plant, thus increasing the proportion of the other particle fractions.

Agglomeration:

Agglomeration refers to the sintering or binding of smaller particles into larger ones. This can lead to a deviation from the optimal particle size distribution and adversely affect operation. In worst-case, so much agglomeration occurs that fluidized bed operation is no longer possible. [15] In the laboratory tests, possible agglomeration was analyzed via the increase in the proportion of particles in the group with the largest mesh size in relation to proportion of the particle of the second sieve. If the mass increased disproportionately in relation to the second particle size classes, agglomeration or other effects of size increasement like e.g., swelling of particles, were assumed, which could have negative impact on operation.

1.1.5 Carrier-specific properties for assessment

Exothermal heat release:

The exothermic heat release represents the amount of heat released by the oxidation reaction of the OC with air in the AR. It is based on the chemical reaction of the reduced metal oxide with oxygen and the energy released by the exothermic reaction and is a guarantee for high temperatures in the AR. On the other hand, this energy proportion must be met in FR to start the reduction reaction of the OC. This leads to an extended temperature spread between the reactors and effects the operation adversely.

Carbon conversion rate:

The carbon conversion X_C directly indicates the capability of an OC in terms of converting char, tar and higher hydrocarbons into measurable gaseous carbon components (CO, CO_2, CH_4). The carbon conversion is therefore an essential attribute of OC in order to achieve high carbon capture rates. This was determined in the laboratory unit via the gas measurements and according to (3. In all experiments ilmenite reached the lowest carbon conversion values. In addition, this value decreases with lower temperatures and more fuel. No deactivation of ilmenite was observed over the five experiments. Initially high values could be related to

available CLOU oxygen of the manganese OC and resulting reduction of this oxygen proportion. This rapid decrease in available CLOU oxygen is known for the most CLOU-capable ores. [16]

CO_2 yield:

The CO_2 yield Y_{CO2} indicates how much of the carbon containing in fuel actually converts to CO_2. This is a characteristic value for complete combustion in the FR and in the laboratory unit. The conversion to CO_2 was higher for manganese-containing OC.

The methane/CO selectivity:

These conversion rates directly indicate capabilities of the OC to convert the species CH_4/CO to CO_2. With these gas components, high reaction rates with the OC are absolutely necessary, since further thermal decomposition of the gases hardly takes place. If the reaction rates for an OC with these gases is low, it could then be necessary to carry out a post-combustion step with oxygen in commercial plants. The so-called oxy-polishing is associated with considerable costs. [17]

Oxygen transport:

The oxygen transport corresponds to the OC's ability to react with oxygen from air and release it accordingly in a reaction with fuel. This property is necessary for CLC operation and is a main marker how much oxygen is available in the FR for fuel combustion.

1.2 Results

1.2.1 Holistic assessment

The laboratory plant experiments and the evaluated parameters provide an overview of the possible performance of the OC. The manganese-containing OC were able to achieve consistently good results for carrier-specific properties. Ilmenite, on the other hand, performs rather moderately in this regard, but stands out due to its excellent bed material properties. When considering the bed material properties of the manganese-containing OC, the values of the Mn ore are especially low compared to the other OC, but those of braunite also reach high values. For the DFB application, it can be said that the operation is more volatile than for simple bubbling beds like the laboratory unit. Therefore, suitable bed materials properties are an important basic characteristic of OC, which are absolutely necessary for successful operation in the 80 kW pilot plant and future

industrial plants. Even with the laboratory unit, operation with the Mn ore as bed material proved to be difficult. Due to the wide particle size distribution and the increased content of fines, a considerable amount of bed material was discharged in a short time. In addition, the low density largely limited the usable gas volume and therefore the experimental conditions. The low bulk density and low heat capacity also would limit the heat transport in a DFB system. If these points are taken into consideration, an increased priority should be given to bed material properties. Braunite achieved almost the same high values for most bed material properties as ilmenite. However, the attrition rate is considerably higher than for other OC and the attrition rate proved to be an important bed material property.

Table 2: OC properties on which the assessment is based with a prioritization of their impact on operation from 1 highest to 3 lowest impacts.

Bed-specific	Effect	Priority	Summary of the reasoning	Limit selection		Unit	Deviation
Density	Heat transport, high FR temperatures	1	Essential for high temperature and stable operation	2400	5000	kg/m³	7%
Bulk density	OC reactor filling, available oxygen	1	Prevent solid circulation and oxygen transport limitations	1000	2500	kg/m³	13%
Particle size distribution	Fine discharge, unstable with coarse	2	Some particle divergence possible, reactor dependency	0.5	0	kg/kg	43%
Attrition resistance	Fine discharge, long-term operation	2	Effect mainly on long term operation	0	0.8	%/h	57%
Agglomeration resistance	unstable operation when to low	3	Effect only with high values, only on long term operation	35	-10	kg/kg	121%
Carrier-specific	Effect	Priority	Summary of the reasoning	Limit selection		Unit	Deviation
Carbon conversion	High carbon capture, low tars	1	No need for CLC without high capture of carbon	60	85	%	18%
CO_2 yield	Quality of combustion	2	Not essential for stable operation, but for efficiency	24	85	%	60%
CH_4 conversion	Higher reactivity for this gas species	2	stable unburnt composition, for less gas treatment	12.5	0	%	55%
CO conversion	Higher reactivity for this gas species	3	Less stable unburnt composition, less treatment	60	0	%	81%
Oxygen transport	More O_2 in FR for combustion	2	Important, compensated by solid circulation and reactivity	-2	25	g	46%
Exothermal heat release	Temperature spread AR, FR	3	Compensated by circulation, density and conversion	5	-1	K/(g* kg)	134%

Based on the overall findings, the properties of the three OC tested in the laboratory reactor were evaluated for their priority by setting limits for each property. Properties with a high priority, such as the density, were assigned with narrow limits. For properties that have less direct influence on operation and the success of experiments in larger plants such as the 80 kW pilot reactor, limits were set at a larger distance from the achieved values of the three OC. A variation of the value of this property has a correspondingly smaller effect on successful operation in the 80 kW pilot plant. The major effects of the parameters on the operation are also shown in Table 2. Although the investigated properties are all important specifications for OC, they have been assigned a priority from 1 to 3 in the table in order to decide the width of the limit selection. The priority level 1 corresponds to effects that are mandatory for operation of the pilot plant. Level 2 has significant impact on stable operation and the combustion reaction, whereas priority level 3 is not essential for stable operation, but can benefit the overall fuel conversion. A brief summary of the reason for the choice of priority level is also provided in the Table 2. As shown in the table, the fluidized bed particle-specific properties are given higher priority, as high values here ensure a basis for stable and successful operation of the pilot plant. The limit values were set depending on the priority level choice at a distance from the measured values. For level 1 the deviation from the upper measured values is up to 30%, level two between 30 and 60% and level 3 above 60%. In order to make the selection of the limits more precise,

tests

were also carried out with quartz sand and synthetic OC (Lana, C28). The exact limits were chosen by evaluating the influence of each limit on the assessment and adjust it based on operation experience with different OC. As the limit values have been selected according to the priority of their properties, the evaluation of the OC can be visualized in so-called spider charts

by depicting every normalized property, shown in Figure 2 and Figure 3. In order to assign a concrete value to the evaluation of the OC, the achieved area in the spider diagram can be calculated for each OC. When comparing with the possible total area, a specific percentage is calculated, which gives a clear comparable value. The area values show that the overall assessment of the three OC is not that different, but also that the three natural ores, ilmenite, braunite and Mn ore with the chosen limits still leave room for improvement. Through pre-treatment e.g., heat treatment or even the production of synthetic OC, the important properties could be directly improved. Practical experience shows that for a value below 30% successful CLC operation is not possible. The assessments of quartz sand on the one hand (no carrier properties) and expensive synthetic OC (Lana) with exceptional good properties for CLC on the other hand show that the area value can at least range with the chosen limits from 10 to 55%.

Up until the report, there has been ten different OC tested with the assessment protocol. Six natural ores, two synthetic OC and one mixture was investigated. The synthetic OC Lana (C28) showed the most promising results, providing an excellent balance between carrier- and fluidized bed specific properties. Of all natural ores, Carajas ore reached the highest area in the spider chart. The high iron content seemed to enhance carbon conversion and reactivity while maintaining good fluidized bed properties. Quartz sand and olivine showed both hardly any oxygen transport and would not be suitable as OC material. The highest CO conversion was reached with the OC with copper contained. This indicates that for full conversion of CO, it is preferred to have a copper concentration in the used OC. The untreated manganese ores, braunite and Mn ore, were especially limited in their fluidized bed properties, also shown in the sub-report about extended analysis. These properties could be highly dependent on the mining area or could be improved by pretreatment. Ilmenite as most common oxygen carrier could convince with it fluidized bed properties and stable operation. By assessment of activated ilmenite (20 h of solid CLC), a shift of area to the left in the spider-chart is shown. This activation and increase of reactivity are known for ilmenite and also discussed in sup-report in regard to phase change and surface. Although this change could be beneficial, the decrease of density, bulk density and attrition resistance have to be viewed critically. A similar shift could be reached by mixing ilmenite with lime. In addition, the lime could enhance catalytic reactions and minimize tar. This was shown by an increased carbon conversion compared to pure ilmenite and activated ilmenite. Mixing natural ores with lime could be simply and cheap way to improve their performance regarding carrier-specific properties.

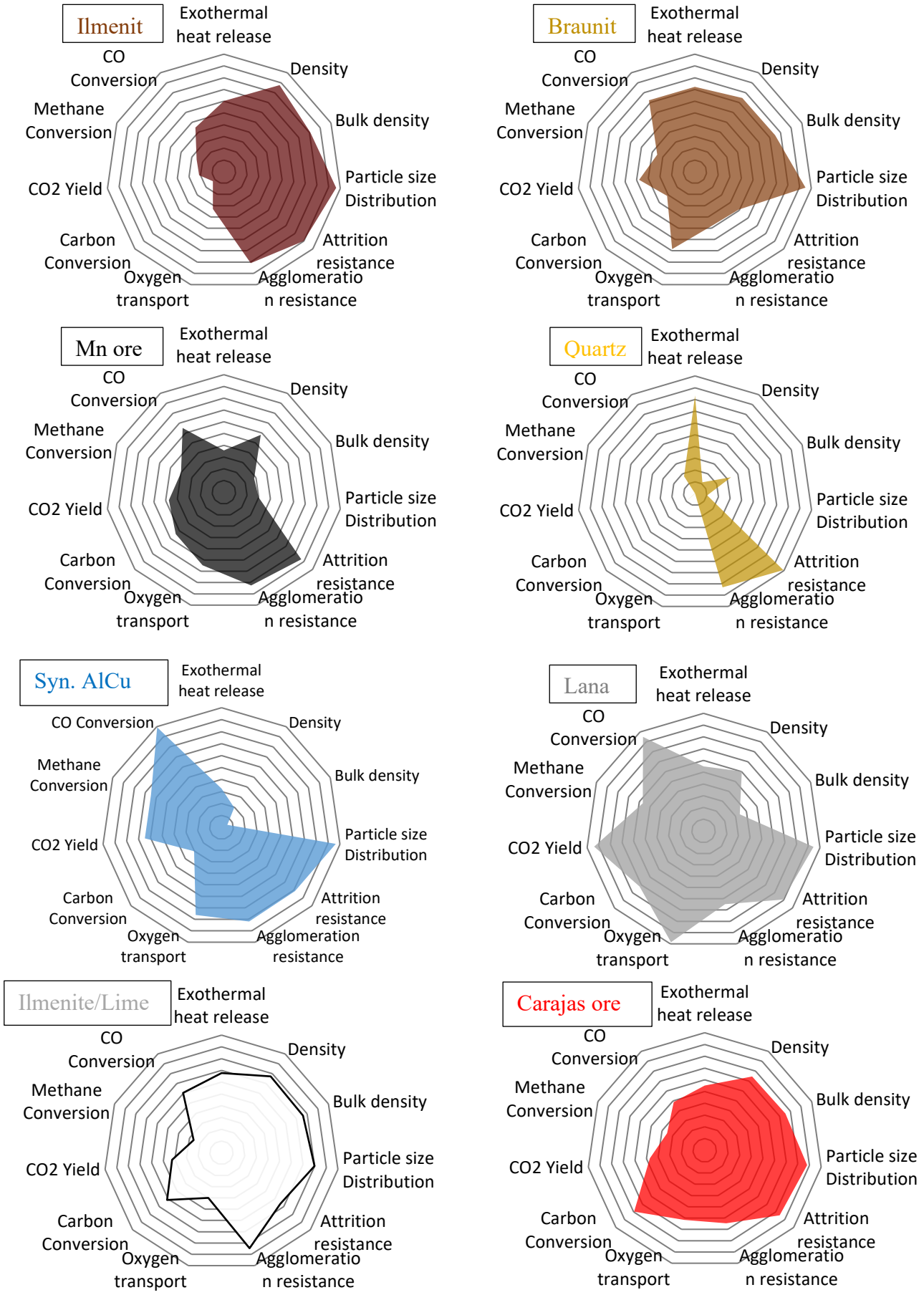

Figure 2: Spider-charts of different oxygen carrier, on the left of each char carrier-specific properties and on the right fluidized bed properties.

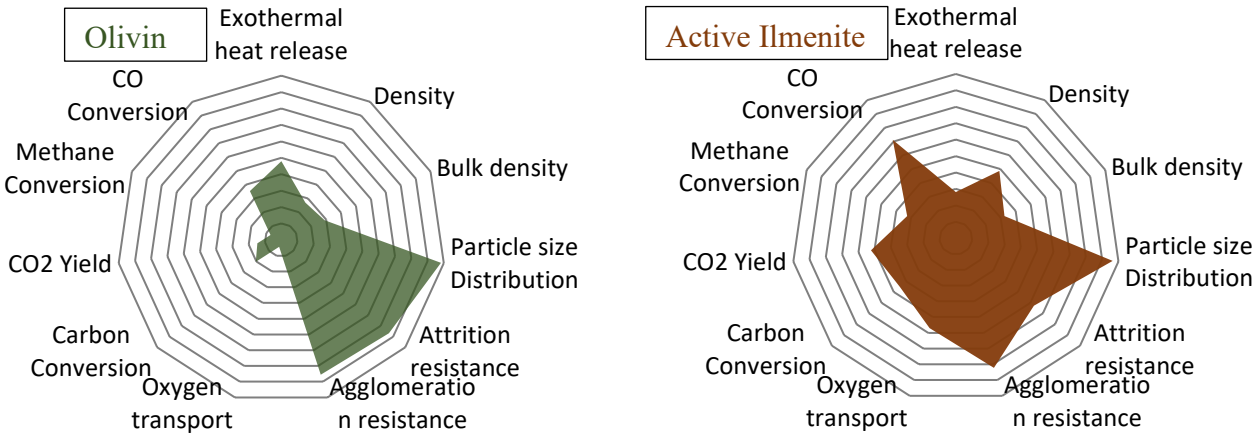

Figure 3: Spider-charts of different oxygen carrier, on the left of each char carrier-specific properties and on the right fluidized bed properties.

1.2.2 First results of long-term experiments

The result of the first long-term experiments shows the reduction of braunite with slow ongoing fuel supply. With lower oxidation state, the fuel conversion of braunite decreased substantially. A significant increase of the attrition rate was also recorded with operation. After the OC is fully oxidized with air, fuel is gradually added. The fluidization takes place with 5 kg/h of steam, while 9.7 g of fuel per reaction cycle is introduced into the reactor. As there is no oxygen supply between the 13 cycles, the braunite should be reduced significantly. Five samples were taken, one in the fully oxidized state and further samples after the 1st, 3rd, 6th and 13th cycle. For taking a solid sample in the reduction phase, flushing with nitrogen is necessary to dry the OC and freeze the oxidation state of the particle. Figure 4 shows the measured oxidation level of the braunite samples. As expected, the measured X_s of the solid samples decreased continuously. After the 6th cycle, the OC releases only small amounts of oxygen, even though X_S only reaches around 60%. Reducing the braunite further, requires higher temperatures or a different reduction medium than chicken manure. However, the oxidized sample ("Oxy") does not reach the full oxidation state, which is defined by heating 24h at 950 °C in an oven. A shorter residence time could be the reason for this. Figure 5 shows the concentration of combustion gases while ongoing fuel supply. Every peak corresponds to one cycle of fuel input. After the sixth cycle, Red 6, a

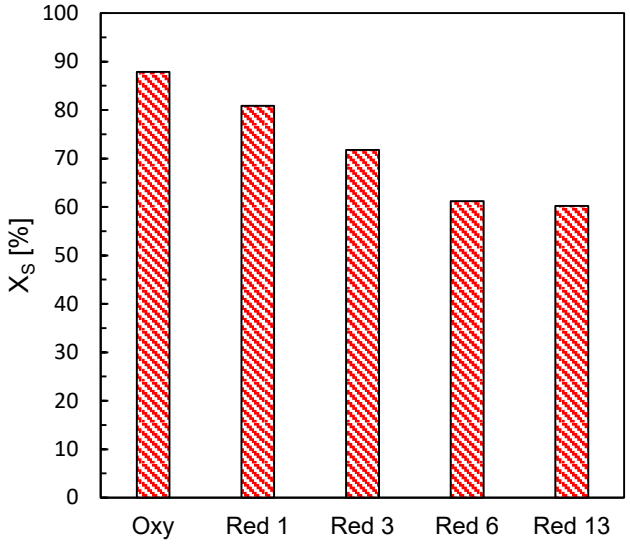

Figure 4: Diagram of the solid conversion X_S of braunite while ongoing fuel supply.

significant increase of the hydrogen concentration occurred. There was no further oxygen available for combustion and the concentration of unburnt gases increases. The experiments showed that the theoretical oxygen transport capacity detected by TGA, will eventually not be reached in fluidized bed with solid fuels. The reason could be that stable phases of the OC can't be reduced with the partial pressures of the reduction mediums. This is not possible in fluidized beds with steam as process medium. In the syntheses of OC for CLC, this effect has to be taken in consideration. Only a small part of the carried oxygen of the OC can be used for combustion. Furthermore, a higher attrition rate was observed with more reduced braunite. The relative high value of braunite even increased and the cyclone was filled extendedly during the experiments.

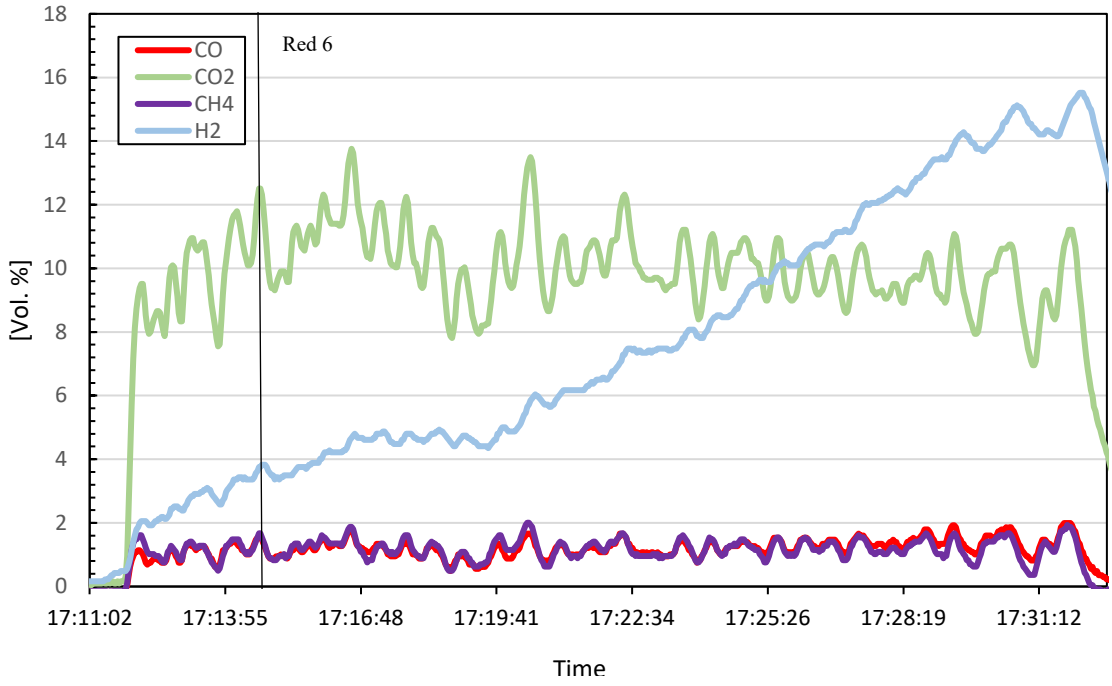

Figure 5: Gas concentrations of the long-term experiment with ongoing fuel supply, braunite as OC.

For the next long-term experiments, the focus should lie on a simulation of the pilot plant operation. The reduction and oxidation reaction of a cycle should correspond as far as possible to the condition in the reactors. This cycle should be repeated as often as possible to get the full picture of cycle stability, long-term attrition rate and possible ash contamination of the bed material, which an all key factors for successful CLC operation.

1.3 Discussion

1.3.1 General recommendations

Important properties are clearly specified by the spider chart and these can be categorized into carrier specific and fluidized bed properties. In addition, some properties increase their leverage with the duration of operation. The suitability of each material depends on the type of feedstock used and the preparation methods carried out. Materials need to be reactive at the process temperatures and environmentally compatible to be suitable feedstocks. Known materials, capable of oxygen transport, include copper, iron, manganese, but only excluding nickel due to

hazardous environmental and health impact. These main components can be supplemented by support feedstock to improve particle properties and activation by catalytic reaction. The materials that have proved suitable for this purpose in the experiments carried out so far are titanium, calcium, magnesium and aluminum. With different mixtures, different properties can be targeted, which can also be further influenced by the processing of the materials. The main goal here should be to achieve high reactivities and oxygen transport while still maintaining the important particle and fluidized bed properties. For example, the stability and abrasion resistance of reactive compounds can be improved by heat treatment or calcination. The duration and temperature of the heat treatment step is essential for the result and can also vary depending on the input materials. In general, there are two feasible methods to attain suitable OC for chemical looping combustion. On the one hand, it is possible to utilize cheap materials like residues or natural ore, which show carrier-specific properties. These can be improved only with basic treatment steps to keep costs down in the process. The resulting OC is probably not reactive enough to fully convert the fuel. This would involve additional costs in reactor optimization and exhaust gas aftertreatment, but inactivated OC can be replaced more easily. On the other hand, is the route of using highly fabricated materials based on synthesis and further processing steps. With suitable choices, an OC can be produced able to fully convert fuel. However, the OC must be designed that the separation from fuel ash is possible or else the costs are probably too high.

1.3.2 Route 1: Natural ores and residues

Route 1 covers the utilization of cheap materials like some natural ores or residues with carrier-specific properties. By using this kind of OC, the fuel will not be fully converted to CO_2. It means that reactor optimization and gas treatment is necessary to maximizes the CO_2 output. Depending on application the CO_2 must have a high purity. In addition to the usual cleaning steps required for a combustion exhaust gas, the oxypolishing process could be necessary for CLC. It is a post combustion process with O_2 as oxidations medium to increase CO_2 purity and reduce unburnt components. The separation of pure oxygen from air which is used in oxypolishing is associated with considerable costs. For this reason, it could be beneficial improving the cheap feedstock by applying pretreatment steps. Mixing different ores could be an example for a simple way of improving some properties of OC. During the experiments, the admixing of limestone to ilmenite could improve fuel, gas conversion and reduce tars. Thereby it is possible to compensate the lack of properties of one ore by adding another one. A mixing for example of ilmenite with braunite could be a good combination with better properties for operation. From an economic point of view, it can also be feasible to perform simple processing steps such as milling, sieving and heat treatment. By milling the OC, the surface and particle size distribution can be adjusted and this can improve reactivity and handling of operation. Sieving of the OC could have impact in a similar way. The hardness and stability of an OC can also be modified by heat treatment like calcination. The effect of the heat treatment is highly dependent on duration, temperature and which stable phases in the OC are formed. On the other hand, the actual positive impact of heat treatment on long-term operation has to be counter balanced to economic factors. The initial hardness and attrition resistance of the OC falls off over the duration of operation and is also highly dependent on the oxidation state of the OC. Moreover, with addition processing steps, the costs of the OC will increase and the advantage of cheap feedstock is lost. A convergence to route 2 takes place and it must be noted that due to attrition, diluting with ash and deactivation, a makeup of OC is necessary in any case.

1.3.3 Route 2: Synthetic oxygen carrier

With route 2 the production of OC is divided in many processing steps so that they refer as synthetic OC. The feedstock material and the different processing steps can be more expensive with the goal of full conversion of fuel to CO_2. The oxypolishing step is with the right OC configuration not necessary. The experiments have shown that for full gas conversion it may be necessary to use high reactive feedstock like e.g., copper. Since the production of OC is expensive, the makeup of OC during operation must be particularly low. The three factors attrition, diluting with ash and deactivation have to be addressed. The attrition resistance is largely dependent on the input materials used, their ratio and the formed phases. The experiments showed so far that iron containing OC have higher attrition resistance than copper or manganese containing OC, but these ingredients are in turn necessary for reactivity. Titanium as support material can improve hardness and attrition resistance, but seem to decrease reactivity. Other support materials that were used during the experiments are Al and Ca, which showed a lower benefit to stability, but perform better in behalf of reactivity than Ti. In addition, the hardness and stability of an OC can be modified by heat treatment like calcination. The effect of the heat treatment is highly dependent on duration, temperature and which stable phases in the OC are formed. A proper heat treatment procedure is much more important than with route 1, because of the high costs of the input material. The diluting of the OC with ash from the solid fuel is even more difficult to deal with. A separation is necessary to minimize the loss of expensive OC and recover it from operation to reintroduce it to the reactor. The common focus is magnetic separation, which is enabled by iron containing phases in the OC retaining ferromagnetic properties. An interesting combination could copper impregnated on an iron-manganese support for ferromagnetic properties and good reactivity. [18] Deactivation, on the other hand, can hardly be avoided. A reduction in surface area, plugging of pores, formation of unreactive phases and ash layer formation occur after long term operation. This makes an investigation of OC in long term experiment important and a possible reactivation by means of heat treatment or removal of the ash layer can also be investigated afterwards.

1.4 Summary project 1

To complete Deliverable 1.1, the methodology developed for characterization and assessment of OC up to Milestone 1.1 was extended and applied to different OC. These were then supplemented by long-term experiments, which were intended to simulate different oxidation states in operation. The experiments resulted in very important properties which have to be properly addressed by the production of the OC. The basic properties can be divided in fluidized bed properties and carrier specific properties. In addition, the properties for longtime operation proved to be also essential. In regard to the findings, two key production routes of OC were defined. The utilization of cheap material with minor production steps or the expensive synthesis of highly complex OC. Subsequently, it is recommended to follow both routes, in the form of mixtures e.g., ilmenite and braunite or a synthesis with copper on a basis of iron-manganese. Another focus should be on optimizing the heat treatment or calcination. In the context of the project new produced OC should be continued to be characterized and investigated in long-term experiments at TU Wien for extended findings.

2 Project 4, Milestone 4.1

Up to this milestone, two experiments on the 80 kW pilot plant were conducted. The objective of the experiments was to investigate different oxygen carrier (OC) and the influence of a variation of temperature and solid circulation of the bed material with biogenic residues as feedstocks. The first experiment used ilmenite mixed with limestone combusting bark pellets as baseline experiment. A controlled variation of the temperature in this reactor set-up was only possible by regulation of the oil injection in the air reactor (AR) to compensate heat loss over the reactor shell. However, the oil injection affected also the CLC operation, because of the decreased oxidation of the OC in the air reactor. This is the reason why variation of the temperature was carried out by comparing operation with oil injection and autothermal operation without oil. In this way, the influence of the temperature and the difference between autothermal operations could be investigated. The second experiment was conducted with synthetic manganese perovskite C28. For purpose of better comparability, the fuel used in this experiment was also biogenic residue in form of bark pellets. For this experiment, the impact of the solid circulation rate was investigated. The solid circulation rate of C28 influenced not only the transported heat from AR to fuel reactor (FR), but also the available oxygen for combustion. The solid circulation rate was controlled by air staging in AR. For a better understanding of the reaction in FR, the gas concentration of the stages of the counter current column was measured. This can be used to assess whether the height/stages of FR are sufficient or an extension will bring additional conversion of unburnt gases.

2.1 Methodology pilot experiments

2.1.1 Reactor concept

Several CLC units can be found in the literature, ranging in scale between the 10 kW_{th} units located at Chalmers University of Technology to a 3 MW_{th} pilot plant that has been erected by Alstom and an 1 MW_{th} pilot plant at Darmstadt University of Technology. [19] Further reactor concepts focus on smaller scale, like an 1.5 kW_{th} demonstration reactor operated by the Spanish National Research Council. [20] Most constructed units have in common the utilization of two interconnected circulating fluidized beds, the so-called dual fluidized bed concept (DFB). The 80 kW pilot plant at TU Wien, see Figure 6, has originally been proposed by Pröll and Hofbauer [21] for solid fuel CLC and Schmid et al. [22] for fluidized bed steam gasification. The pilot plant (design load 80 kW_{th}) consists of two circulating fluidized beds which are connected at the top and bottom via steam fluidized loop seals. The AR is designed as fast fluidized bed with an inner diameter of 125 mm. Air can be introduced at

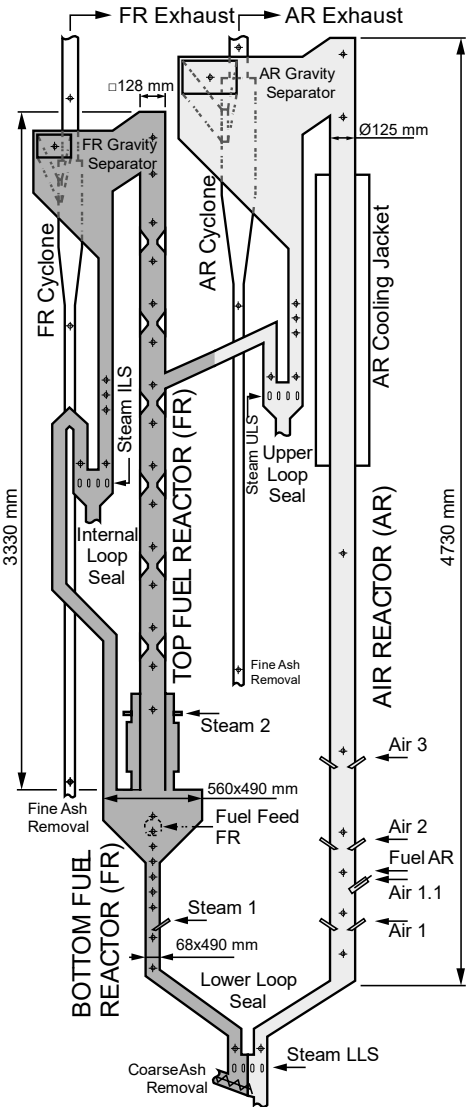

Figure 6: Scheme of the 80 kW_{th} pilot plant at TU Wien.

three different levels. The solids circulation of oxygen carrier between AR and FR is mainly controlled by the AR fluidization rate, where air is used as fluidization medium. Solids entrained from the AR are separated by a gravity separator with gentle separation characteristics and transported to the FR via the upper loop seal (ULS). Using this setup, solids circulation between AR and FR is only controlled by AR fluidization and solids entrainment respectively. The FR is divided into two different parts: The lower part is designed as bubbling fluidized bed with high solids inventory to ensure proper solids residence time and char gasification. The subsequent upper part of the FR has internals placed along its height, reducing the free cross section of the reactor. The internals disturb the formation of the core-annulus profile and intensify the gas-solid contact by increasing the solids hold up [23]. The free cross section area of the internals can be adjusted between 20.3 and 35.6%. Due to the gas velocities in the upper part of the FR, a counter-current flow between gas and solids is obtained with minimal solids entrainment. The FR is fluidized by steam, which can be introduced at the bottom of the reactor and above the lower part. Entrained solids are separated by a gravity separator and returned to the bottom FR by the internal loop seal (ILS). The solids loop to the AR is finally closed by the lower loop seal (LLS). Additionally, AR and FR are equipped with high efficiency cyclones for secondary solid separation of fine particles. The fuel is fed into the FR above the bed surface via a screw feeder. Auxiliary fuel in form of fuel oil can be introduced to the AR to compensate for high heat losses caused by the large specific surface area of the plant. The exhaust gas stream of the two reactors were continuously monitored with respect to O_2, CO_2, and CO (AR) as well as CO_2, CO, CH_4, H_2 and O_2 (FR) with Rosemount NGA 2000 gas analyzers (UV/IF, paramagnetic and heat conductivity). In addition, gas chromatography was used to determine N_2 in the FR exhaust gas.

The pilot plant has been originally designed for dual fluidized bed gasification and is in operation since 2015 [24]. Work included investigations with different fuels and different bed materials [5, 25-27]. The First solid CLC experimental Campaign was conducted and published in 2018. [28]

2.1.2 Materials and characterization

Ilmenite, a natural iron titanium ore, was used as oxygen carrier (OC) for the first experiment of the campaign, since it can still be considered as the most researched benchmark material for solid fuel CLC. It is a so-called heterogeneous OC, i.e., it is not able to release gaseous oxygen and fuel conversion happens solely via gas-solid contact. The material was supplied from Norway and particles had a diameter d_{sv}=*150 µm*. The composition can be found in Table 3. It was mixed with 20% of limestone $CaCO_3$, which after calcination to CaO accounted for about 10% of the bed mass. The characterization and assessment of the materials, which was elaborated in Project 1.1 is seen in Figure 7. [29] It can be seen that the mixing with lime shifted the OC to better carrier-specific properties like conversion of gas and carbon.

Table 3: Composition of the Norwegian ilmenite (components >0.1 wt%).

Content [wt%]		Content [wt%]		Content [wt%]		Content [wt%]	
TiO_2	44.08	MnO	0.30	O with Fe	11.36	S	0.14
Fe^{2+}	25.93	CaO	0.32	MgO	3.58	Cr_2O_3	0.10
Fe^{3+}	9.14	V_2O_3	0.17	SiO_2	1.99	Al_2O_3	0.64

The OC used for the second experiments of the campaign is Lana, also called C28. The spray-dried material is a CLOU type oxygen carrier, releasing oxygen at conditions with low oxygen partial pressure. The material has a perovskite structure and a composition of $CaMn_{0.775}Mg_{0.1}Ti_{0.125}O_{2.9}$. The OC used in this campaign has been produced by Euro Support

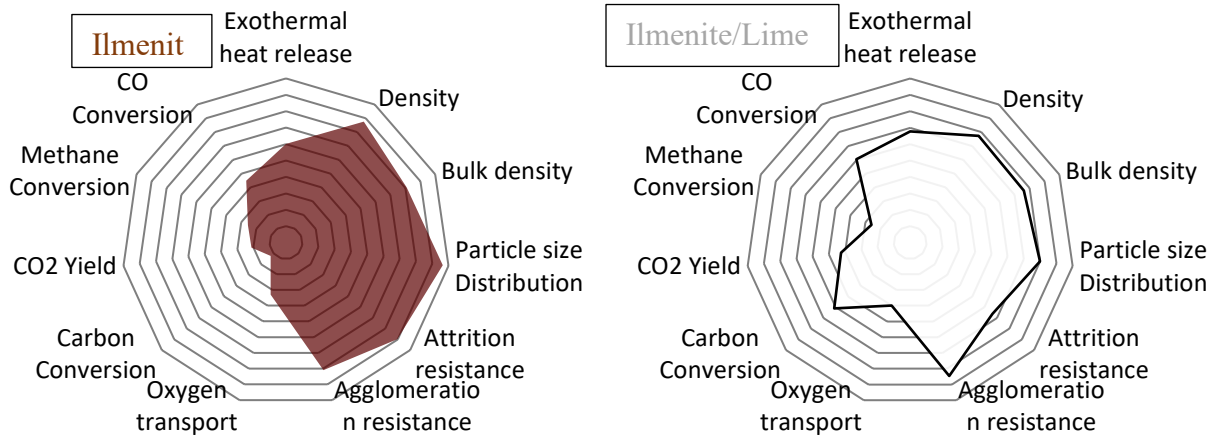

Figure 7: Characterization and assessment of ilmenite and in comparison, ilmenite mixed with CaO.

Advanced Materials (ESAM) and is left over material from the gas CLC project SUCCESS. Important details are given in Table 4.

Table 4: Detailed information about Lana/C28 produced by ESAM in the framework of the SUCCESS project.

	(Product Name/Reference) Finished Product	
Chemical Composition	**Target**	**Method of analysis**
Mn3O4	48 wt%	XRF (semi quantitative)
CaO	41 wt%	XRF (semi quantitative)
TiO2	8 wt%	XRF (semi quantitative)
MgO	3 wt%	XRF (semi quantitative)
Physical test methods		**Method of Analysis**
Tapped density	1.6 - 1.7 g/mL (hollow spheres) 1.7-1.8 g/mL (solid spheres)	Quantachrome Autotap
Phase composition	>95% perovskite	XRD
Particle size	D10: 90 - 130 µm D50: 140 - 180 µm D90: 190 - 230 µm	Mastersizer 2000 (light scattering measurement)
Physical Characteristics		
Appearance	Dark grey sand like powder, free flowing	
Particle shape	Spherical (optical microscope)	

The material, called C28, was originally developed by Chalmers University of Technology and VITO [30]. Addition analysis of the fresh OC material used in this study is shown in Table 5. The particle size distribution was measured by means of a laser diffraction technique with a

Malvern Mastersizer 2000. The formed crystalline phases were analyzed by X-ray powder diffraction (XRD) using a Philips X'Pert diffractometer with PANalytical X'Pert Pro software and oxygen transport capacity was determined by thermogravimetric analysis, see Table 5.

Table 5: Physical and chemical properties of the fresh OC

Parameter	Value
XRD main phases	$Ca((Mn_{0.9}Ti_{0.1})O_{2.961}$, MgO, $CaMn_2O_4$
Mean particle size [µm]	139
Bulk density [kg/m³]	1780
R_O Oxygen transport capacity [kg/kg], [3]	0.08

The synthetic OC was also characterized in project 1.1 and reached consistently high values in nearly all properties, see Figure 8. The OC showed the best carrier-specific properties of all OC tested so far. Only the synthetic copper OC reached higher CO conversion rates.

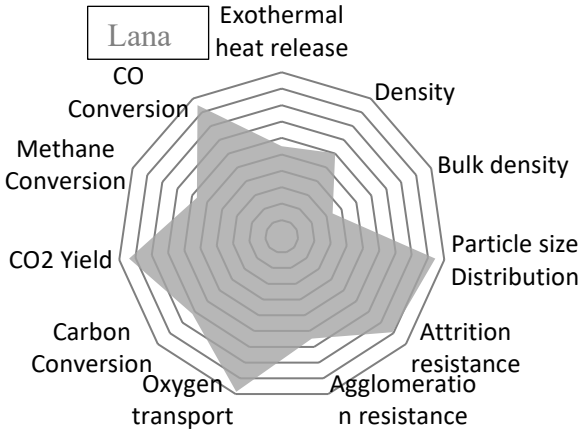

Figure 8: Characterization and assessment of Lana/C28.

The used fuel was bark pellets made from commercially available bark mulch. It was first grounded and then processed in the pelletizing machine with the addition of a small amount of water. After drying the resulting pellets had a diameter of about 6 mm and a length of 5-40 mm. The fuel analysis is given in Table 6. For heat up and reference operating points, softwood pellets were used of class EN-plus A1 according to ISO 17225-2 as fuel. These pellets are characterised by a low ash content and sulphur/chlorine content, which is important for the experiments, because less interference based on ash and fuel contaminations occur.

Table 6: Fuel analysis of the used fuels.

		Softwood	Bark Experiment 1	Bark Experiment 2
Water content	wt%	7,2	5.3	16,1
Ash	wt%(wf)	0,2	11.5	17.4
Carbon	wt%(wf)	50,7	47.1	45.03
Hydrogen	wt%(wf)	5,9	5.0	3.4
Oxygen	wt%(wf)	43,0	35.8	35,5
Nitrogen	wt%(wf)	0,2	0.6	0.7
Sulphur	wt%(wf)	0,0	0.05	0.06
Chlorine	wt%(wf)	<0,01	<0.01	<0,01
Volatiles	wt%(waf)	85,4	70.5	69,9
LHV (dry)	kJ/kg(wf)	18900	16900	16400

The bark pellets of experiment 2 were also characterized by their ash behaviour and composition. The high ash melting behaviour should be sufficient for CLC operation and XRF-analysis show high concentration of Si, Ca and K, see Table 7 and Table 8.

Table 7: Ash melting behavior of the bark pellets of experiment 2.

		Bark Experiment 2
Softening point	°C	1160
Hemisphere temperature	°C	1230
Flow temperature	°C	1390

Table 8: Elemental ash composition of the bark pellets of experiment 2.

Element	w%	Element	w%
Mo	0.2	Cr	0.1
Nb	0.2	V	0.1
Zr	0.2	Ti	0.5
Sr	0.2	Ca	11.9
Pb	0.1	K	7.2
As	-	Cl	0.2
Zn	0.1	S	0.2
Cu	0.1	P	0.3
Ni	0.1	Si	23.4
Co	0.1	Al	6.1
Fe	2.7	Mg	1.2
Mn	0.6	Na	1.6
O	42.6		

2.1.3 Data evaluation and modelling

Mass and energy balance modelling and data evaluation was performed using the simulation software IPSEpro by Simtech Simulation Technology. It is a stationary, equation oriented software for the simulation of power and chemical plants and can be used for quick, preliminary process evaluation, detail engineering and design, monitoring and optimization of existing

plants as well as for statistical validation of measurement data. The big advantage of IPSEpro is its modular structure (see Figure 9) giving the user full control over the whole simulation process. This includes full knowledge about the used models and property data without limitations in expanding existing models and libraries. Such an approach is very valuable in research and development, especially for processes at an early stage of development, as it is the case for CLC.

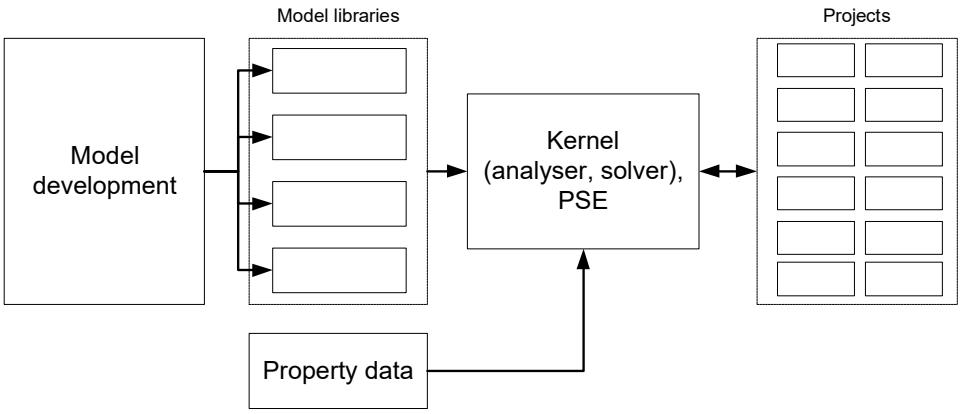

Figure 9: Structure of the process simulation software IPSEpro.

Standardized components, so-called units, are formulated based on mathematical equations and variables. These units are stored in the different model libraries and equations are formulated in a way that mass and energy balances are strictly fulfilled for each unit. IPSEpro's user interface (Process Simulation Environment, PSE) is used to build the model, or flow sheet, of a complete process out of the units (the project). This process model is used together with the property data to build a single system of (non-linear) equations which is numerically solved using the Newton-Raphson method.

IPSEpro can also be used for verification of measurement data based on closing mass and energy balances of a modelled plant. This requires mean values of measurement data (pressures, temperatures, flow rates, gas concentrations, etc.) for a certain time interval during steady state operation of the investigated plant. The set of measured data is used together with the process model to create an over-determined system of equations, i.e., it has more equations than variables. Additionally, a tolerance is assigned to each measurement value reflecting its quality and deviations during the observed time interval. This overdetermined system of equations can be solved using the method of Lagrange multipliers resulting in a least squares problem for the deviation between measured value and balanced solution:

$$\sum_i \left(\frac{x_i - \bar{x}_i}{tol_{x_i}} \right) \rightarrow Min$$

The balanced solution of the measurement data reflects the most probable operation condition of the investigated plant within the model structure fulfilling mass and energy balances.

In the model, AR and FR are each modeled as a single balance zone and the solid OC is circulating between them, see Figure 10. The in- and outgoing gas streams of each reactor are summarized prior to entering the reactor including fluidization gases of the loop seals. Here, LLS fluidization is fully included in the gas stream entering the AR and the fluidization streams

of ULS and ILS are completely added to the streams entering the FR. The model also allows intermediate access to performance parameters based on fuel conversion. In the present work, solids circulation between the two reactors is not measured but calculated based on reactor temperatures, gas conversion and solids conversion.

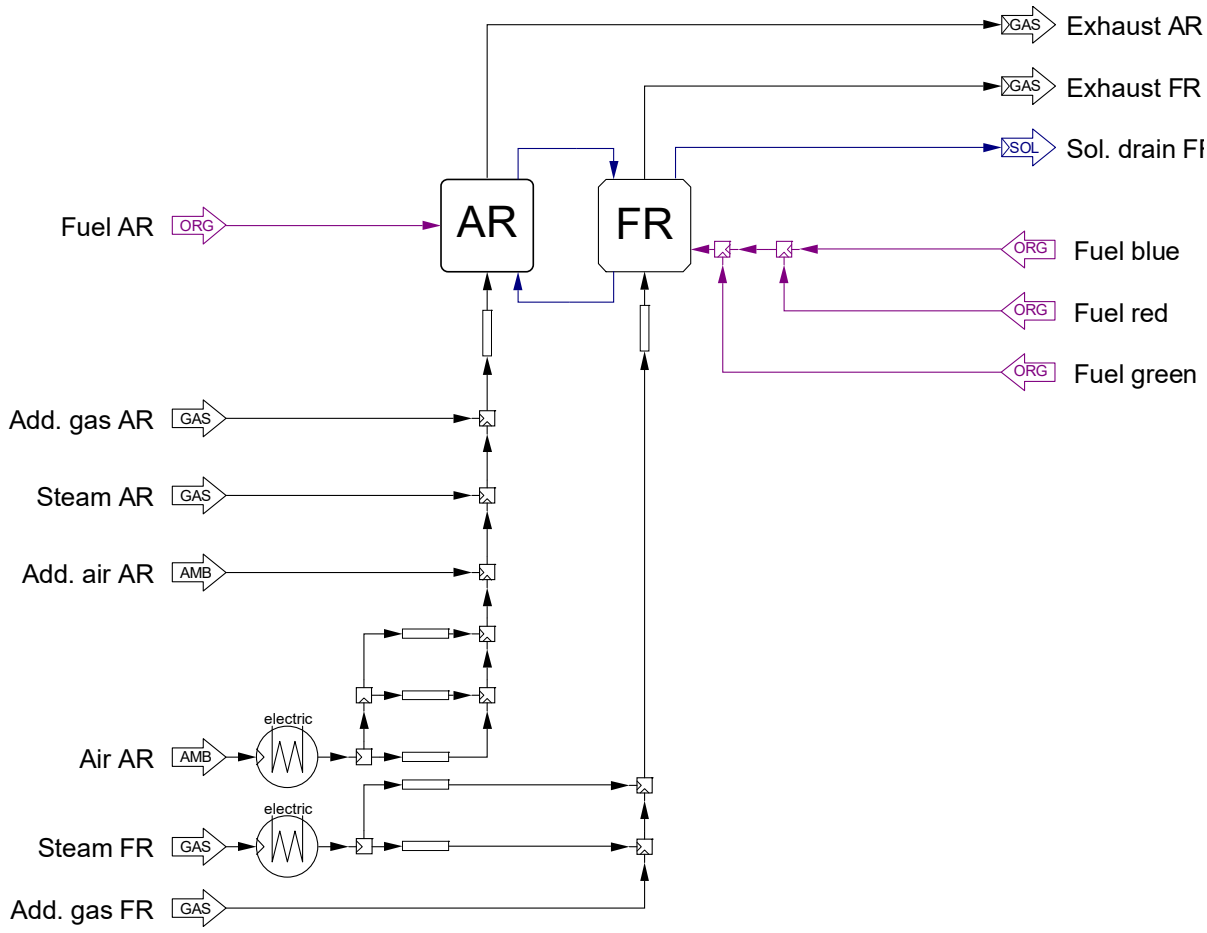

Figure 10: Basic model of the 80 kW CLC pilot unit.

2.1.4 Experimental setup and evaluation

A detailed description of the experimental setup and procedure is given by Penthor et al. (2018). Every experimental point was operated with constant condition for at least 30 minutes. The goal of every operating point has always been to achieve stable operations with the highest possible conversion to CO_2. In order to have a clear overview of the experimental conditions, there are several temperature and pressure measurements spread over both reactors. In addition, the gas concentration of the exhaust gases from Fr and AR are measured. In the AR exhaust gas CO_2, CO and O_2 are measured. In the FR exhaust gas, a gas chromatographic measurement is carried out in addition to a constant measurement of the concentration of gases. The gases measured include O_2, CO_2, CO, CH_4, H_2, N_2, C_2H_2, C_2H_4 and C_2H_5. Based on the available measurements and the known input flows, a complete mass- and energy balance could be calculated for each experimental point with the software Ipse pro. To evaluate and assess the performance of the OC and the operating point in the plant, important parameters can be observed. The carbon capture rate η_{CC} describes how much of the carbon introduced into the fuel reactor is found in the gas phase of the fuel reactor exhaust gas. This also represents the loss of carbon, mainly through combustion in the air reactor.

$$\eta_{CC} = \frac{\dot{n}_{C,FR,exhaust}}{\dot{n}_{C,FR,feed}} \cdot 100 \quad [\%] \quad (6)$$

The CO_2 yield γ_{CO2} describes how much of the carbon introduced into the fuel reactor is contained in the fuel reactor exhaust gas as CO_2. It is a measure of incomplete conversion of the fuel carbon to CO_2:

$$\gamma_{CO_2} = \frac{\dot{n}_{C,CO_2,FR,exhaust}}{\dot{n}_{C,FR,feed}} \cdot 100 \quad [\%] \quad (7)$$

The CO_2 selectivity S_{CO2} describes how much of the carbon of fuel reactor exhaust gas is in the CO_2 stream. It is an even better measure of incomplete conversion of the carbon to CO_2:

$$S_{CO_2} = \frac{\dot{n}_{C,CO_2,FR,exhaust}}{\dot{n}_{C,FR,exhaust}} \cdot 100 \quad [\%] \quad (8)$$

The Combustion efficiency η_{Comb} describes how much of the fuel is actual converted to CO_2 and H_2O. It combines the unconverted gases with the lost fuel to the AR reactor and gives an overall assessment of the CLC operation. It is based on ratio of the demanded oxygen for complete stoichiometric combustion of the exhaust gas $\dot{n}_{O_2,fuel,dem}$ and of the fuel $\dot{n}_{O_2,fuel,dem}$.

$$\eta_{Comb} = (1 - \frac{\dot{n}_{O_2,exhaust,dem}}{\dot{n}_{O_2,fuel,dem}}) \cdot 100 \quad [\%] \quad (9)$$

The total Oxygen Demand ΩOD describes the amount of oxygen necessary for complete oxidation of the FR exhaust gas compared to the amount of oxygen necessary for full oxidation of the fuel feed:

$$\Omega_{OD} = 100 - \eta_{Comb} \quad [\%] \quad (10)$$

2.2 Results and discussion

2.2.1 Operation of experiment 1, ilmenite/lime

The start-up procedure of the pilot plant was divided into two different phases: During the first phase, the fluidization of the AR and FR (air for both reactors) was preheated up to 700 °C using electrical heating. When the plant temperature reached 400 °C, fuel in form of light fuel oil (AR) and soft wood pellets (FR) was fed into the plant. At 900 ° C, the air fed to the FR was gradually replaced by steam (at around 12:45) to initiate CLC operation, see Figure 11. Then the ramp-up of temperature and gas conversion started by optimizing the operation condition and warming up of the steel housing. At 17:00 the fuel of the FR was changed from wood pellets to bark pellets and the ramp-up was continued. The green area marks operation with stationary condition with only minor changes in temperatures, concentrations and material transport. OP1 was the first operation point reached with stationary conditions and oil addition the AR. Thus, high temperatures in both reactors and CO_2 concentration up to 88% were achieved. While in OP2 the temperature in both reactors decreased while higher CO_2 concentrations were reached. This operating point was carried out with no addition of oil in the AR, which means autothermal condition and was also characterized by lower temperature fluctuations in the AR. The temperature of the AR was kept with the exothermal oxidation reaction of the OC alone at this high level. Overall, the operation was highly stable, although the solid circulation rate was hold close to maximum, right before flooding of the

counter-current column of the FR could occur. The grey areas do not show an impairment of operation, but a change in the location of gas measurement and the swap of fuel from wood to bark.

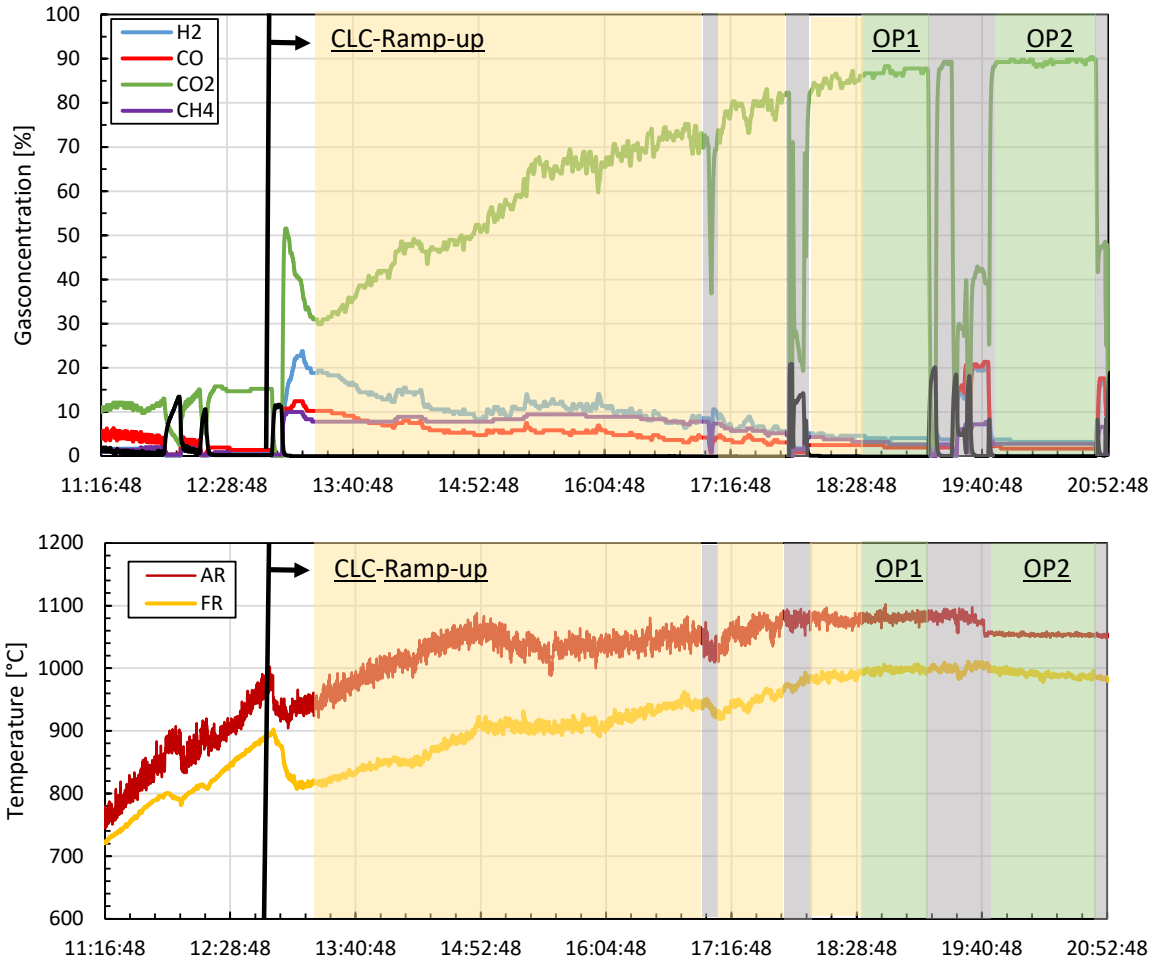

Figure 11: Gas concentration of FR exhaust and temperatures over the duration of the experimental day.

2.2.2 Stationary operating points of experiment 1, temperature variation

During operation two stationary operating points were achieved, OP1 and OP2. For both operating points applied that the process conditions were not changed for at least half an hour, resulting in only minimal changes in temperature and gas concentration. Of all the values, the temperature in the FR changed the most during OP2. The high heat losses through the reactor and the autothermal operation causes a drop in temperature, which would level off if heat loss and generated heat were balanced. Because the concentration of the gases in the FR were not impacted by the temperature drop and the experimental time was limited, it was decided not to wait until the temperature was levelled off. For reactors of higher scale, heat loss would be considerably lower due to better insulation and reactor lining. Moreover, the temperature of the AR would be adjustable by cooling through the wall by steam production. Figure 12 presents the average temperature profile over the reactor, AR and FR, of both operating points. In general, 10 to 20 °C higher temperatures were achieved at OP1, but the largest difference in temperature was measured in the AR between a height of 1 and 2 m. This resulted from the placement of the oil injection and the heat release due to combustion. In the

temperature profile of the FR, the energy demand of the gasification of the fuel is clearly visible. In the conical bubbling bed of the FR, the temperature decreased over 100 °C. High

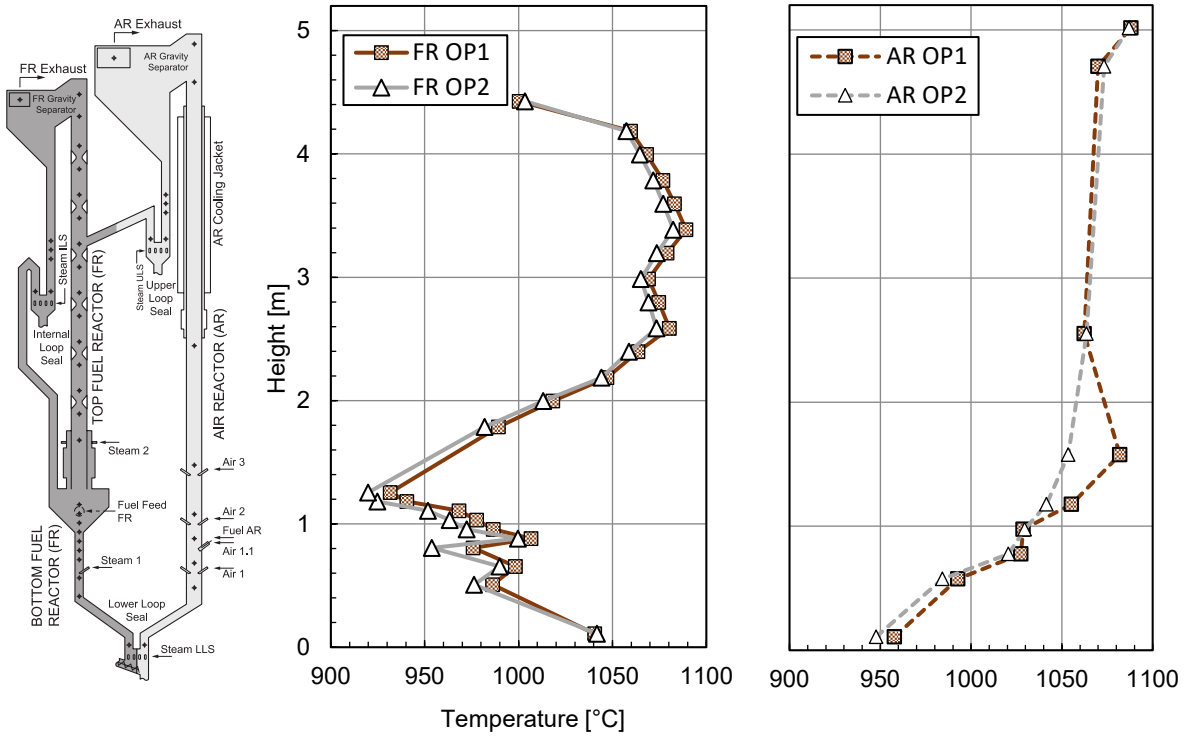

Figure 12: Temperatures over the height of both reactors, AR and FR, of OP1 and OP2.

temperatures in this part of the reactor are essential to favor gasification speed and therefore minimize carbon loss to the AR. In the upper part of the FR the temperature increased due to the combustion of the gasification gases and the inlet of hot OC from the AR. In this part the temperature difference of the operating points dwindled because of higher gas conversion of OP2. Beside the temperatures, the solid circulation and the OC distribution have most impact on the operation in the pilot plant. Higher solid circulation of OC leaded to more heat transport to the FR and more available oxygen for combustion. The solid circulation rate is controlled by the air flow of the AR and by air staging, see

Table 9. Figure 13 shows that higher solid circulation rate SCR of OP1 leads to more material in the lower part of FR and less material in the AR, given in a zeroed pressure drop in over the reactors. The addition OC in bubbling bed and with the higher temperatures of OP1 benefited the gasification reaction of char and resulted in higher carbon capture compared to OP2. Also the countercurrent column was slightly more filled with OC in OP1, but this did not result in higher CO_2 concentration, mainly because the fuel addition was also increased compared to OP2.

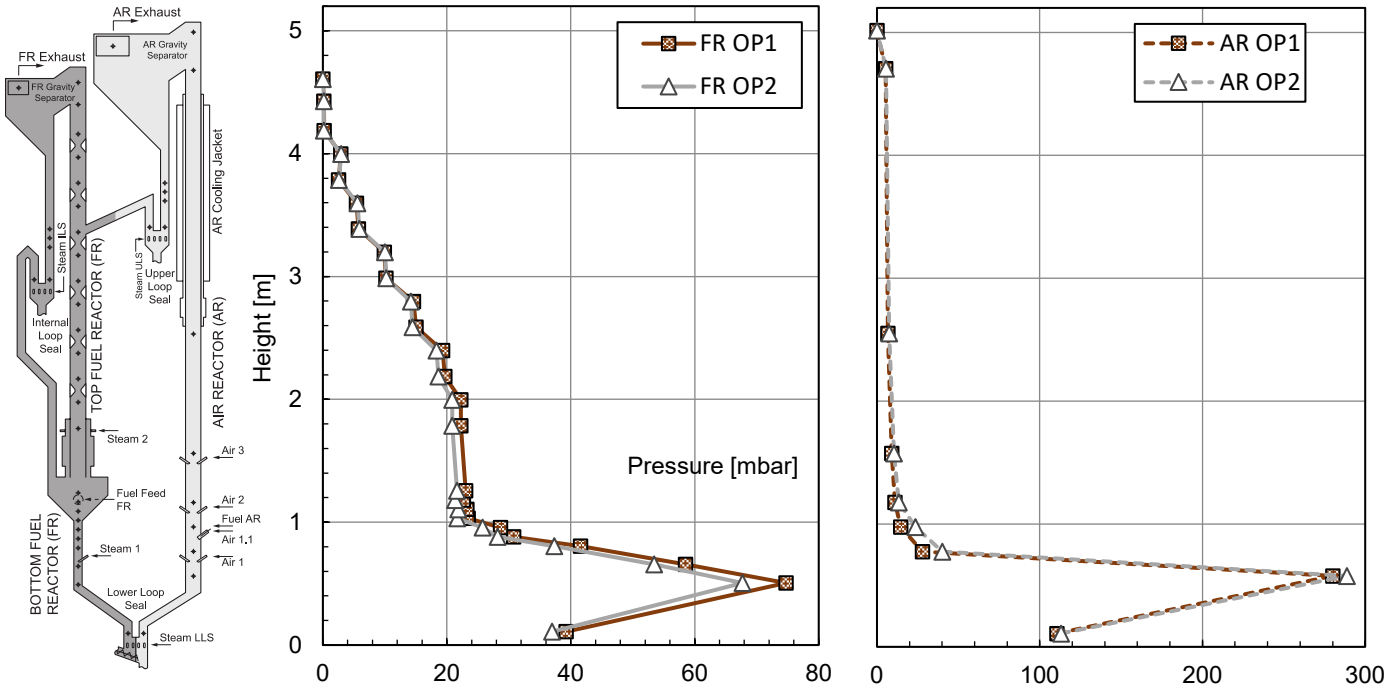

Figure 13: Pressure over the height of both reactors, AR and FR, of OP1 and OP2.

Table 9: Air staging resulting in different solid circulation rates of OP1 and OP2.

	V_AR_sum [Nm³/h]	V_AR_prim [Nm³/h]	V_AR_sec [Nm³/h]	V_AR_tert [Nm³/h]	Rest [Nm³/h]	**SCR [kg/h]**
OP1	94.9	31.5	40.8	17.6	5.0	**1503.6**
OP2	72.5	17.4	30.1	19.9	5.1	**1138.1**

Figure 13 also indicates that the upper third of the countercurrent column contained hardly any OC. This leads to the assumption that only a part of the upper FR participates in the inhomogeneous gas-solid reaction necessary for combustion in CLC. Although no higher hydrocarbons were measured by the gas chromatography in both operating points, Figure 14 shows that the fuel conversion was not complete. When comparing the operating points, OP2 had lower gas concentration of CO and H_2 as well as a lower tar loading in the FR exhaust gas. The reason for this can be attributed to higher fuel addition resulting in higher gas velocities, higher solid circulation with less residence time in the reactors and a possible lesser oxidation grade in the AR also due to the oil injection. In contrast the higher temperature of OP1 could benefit the decomposition of CH_4 to smaller gas components. By comparison the assumption could be made, that longer residence times would bring the operation closer to full combustion. In case of reactor design a longer counter current column or the OC inlet at a higher point of the reactor would promote gas conversion. When setting parameters in DFB, especially in autothermal operation, it must be added that the operation conditions have major influence on each other. That means for example that a change of solid circulation rates also affects the temperature in both reactors, but likewise has the temperature impact on the solid circulation

by changing the gas velocity. This behaves similarly with the conversion of char and gas which is also most influential on the temperature. In this respect, a more in-depth interpretation of the

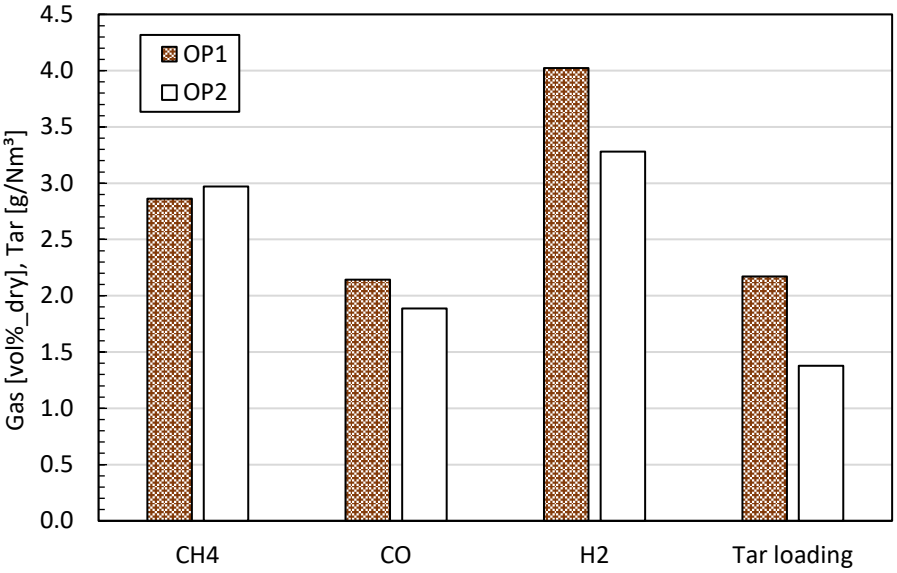

Figure 14: Concentrations of unburnt gas components and tar loading of FR exhaust gas.

operation than here would require considerably more different experimental points and thus more operating time.

The slip of carbon to the AR was determined by the measurement of the exhaust gas. Due to the oil injection in OP1 the CO_2 concentration of the AR exhaust gas is higher than in OP2. By balancing the carbon carried by air fluidization and injected by oil, the carbon capture rate of the operated point could be calculated, see Table 10. The carbon injected by oil is not included in the carbon capture rate, because the oil is for compensating heat loses, which would not be necessary in scaled reactor with sufficient insulation. The oil injection decreases the accuracy of the carbon capture rate, because another dependent variable is added and small alterations of CO_2 concentration represent major changes in total carbon resulting by the large volume of the AR exhaust gas stream.

Table 10: Carbon capture rate and important parameter of the carbon balance in the AR.

	AR air input [Nm³/h]	CO_2 exhaust gas dry [%]	O_2 exhaust gas dry [%]	Light oil mass flow to AR [kg/h]	Carbon capture rate [-]
OP1	94.9	3.10	4.95	1.51	99.5
OP2	72.5	0.82	7.06	-	95.8

2.2.3 Comparison with pure ilmenite

A recent experimental campaign on this plant was conducted with three different OC and five different fuels. As comparison the results of pure ilmenite and pelletized bark are of interest for these experiments. Table 11 shows the important experimental parameters and results. When considering the performance parameters like the carbon capture rate, the CO_2 yield or the combustion efficiency, an increase of all three with the ilmenite/lime mixture is shown. The main difference is the concentration of unconverted gases of the exhaust gas like CO, CH_4 and

H_2 resulting in this gab of the CO_2 yield between the experiments. There were also higher loading of tar and higher hydrocarbons measured with pure ilmenite as OC.

The operating conditions of the different experiments already clearly indicate why the performance of OP1 and OP2 turned out to be higher. On the one hand, the power input to FR was lower during the experiments with lime. A higher solid circulation rate was thus necessary to transport sufficient heat and oxygen. This also resulted in a lower steam to carbon ratio in the FR, which was disadvantageous for the gasification reaction of fuel. On the other hand, the general temperature during the experiments was higher. For example, the temperature of the exhaust gas streams of each reactor was around 150 °C higher with lime. One reason for this was the addition of oil in the AR to compensate for heat losses during OP1. Without oil addition, also the temperatures during OP2 started to drop slightly. You can see from the curves that the temperature of the FR is already close to levelling off. The constant temperatures in the AR also indicate this, since in the DFB system the reactors are in equilibrium and the instant temperature drop in the AR by turning off the oil continued in the FR over some time. This means the temperatures reached with autothermal process conditions were way higher with ilmenite plus lime triggered by higher conversion of tar and gases in the FR reactor. A catalytic effect initiated by lime benefits the water-gas shift reaction converting CO and H_2O to CO_2 and H_2, which is more reactive with ilmenite. [31, 32] Higher temperatures in the FR favor the oxygen release of OC, which also benefits the gas conversion. That means although the total oxygen transport capacity of the ilmenite lime mixture is lower than of ilmenite, it is capable of realizing enough oxygen for higher gas conversion rates. With the results achieved, not only the previous experiments with bark were surpassed, but also the highest CO_2 yield and combustion efficiency were achieved so far in this reactor setup. The rate of full converting the gases to CO_2 decreases in general with the fuel concentration of volatiles. [33] High combustion efficiencies over 90% with high concentration of volatiles like with bark, are normally only reached with more reactive OC, for example copper ore, manganese ore or synthetic OC. These highlights both the importance of the counter current column for improved gas solid contact and as well the blending of ores for a boost of reactivity. Nevertheless, by utilization of available natural ores or residue materials, full gas conversion to CO_2 wasn't reached yet. For commercial plants, a concept for further treatment of the exhaust gas must be available.

Table 11: Comparison of OP1 and OP2 with a former experimental campaign with ilmenite.

Operating point name	Bed material	Fuel blue hopper	Fuel power input FR	Fuel power AR oil	OC to fuel ratio	Mean global solids mass flow	Carbon capture rate	CO_2 yield	Comb. Efficiency	Steam to carbon ratio	O_2 demand	Temp. AR	Temp. FR
			P_fuel_FR	P_oil	φ_OC	ms	ηCC	γCO_2	ηcomb	S/C	Ω_{OD}	ϑAR_{exh}	ϑFR_{exh}
[Text]	[Text]	[Text]	[kW]	[kW]	[-]	[kg/h]	[%]	[%]	[%]	[-]	[%]	[°C]	[°C]
OP1	Ilmenite/Lime	Bark	71.8	17.6	3.0	1503.6	99.5	93.3	91.0	1.4	9.0	1088.0	1059.7
OP2	Ilmenite/Lime	Bark	62.0	0.0	2.7	1138.1	95.8	90.3	91.7	1.5	8.4	1087.0	1057.5
Rinde_1.1	Ilmenite	Bark	77.7	0.0	3.2	1726.2	94.9	82.9	81.9	1.1	18.1	915.7	920.2
Rinde_1.2	Ilmenite	Bark	78.2	0.0	3.2	1733.5	95.2	85.4	82.6	0.8	17.4	913.7	913.1

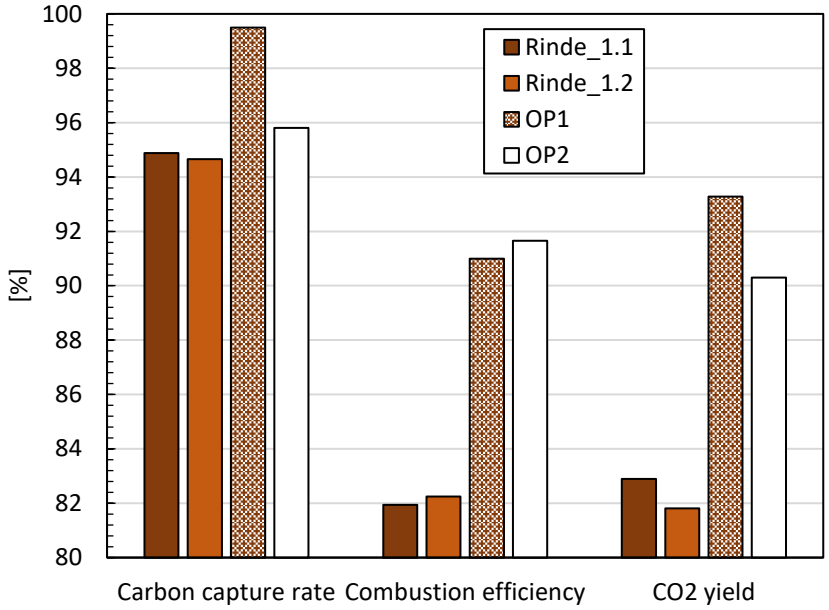

Figure 15: Results of the experimental campaign on the 80 kW pilot plant, comparison of results of ilmenite to ilmenite mixed with lime.

Vienna, 25.03.2022

2.2.4 Operation of experiment 2, Lana

The second experiment consisted of two experimental days. The first day included heat up and the variation of the solid circulation rate, see Figure 16. On the second day, gas concentrations over the countercurrent column of the FR were measured to determine the influence of height and constriction on gas conversion. The operation with the synthetic OC Lana was stable and duration of heat up was shorter than with Ilmenite. While heating up some problems with the gas measurement occurred, see red marked timeframe, and unfortunately this was the reason that both reactors were operated at reduced atmosphere for some time, because of incorrect values were displayed. Although the CLC process then worked without problems, it is possible that the OC was damaged. This can result in reduced reactivity and attrition resistance. Increased attrition was indeed detected during the experiment, although it lacks reference experiments to quantify the statement. The green marked area symbolizes steady state operation. After the first green area at around 17:20 the fuel was changed to bark pellets. This

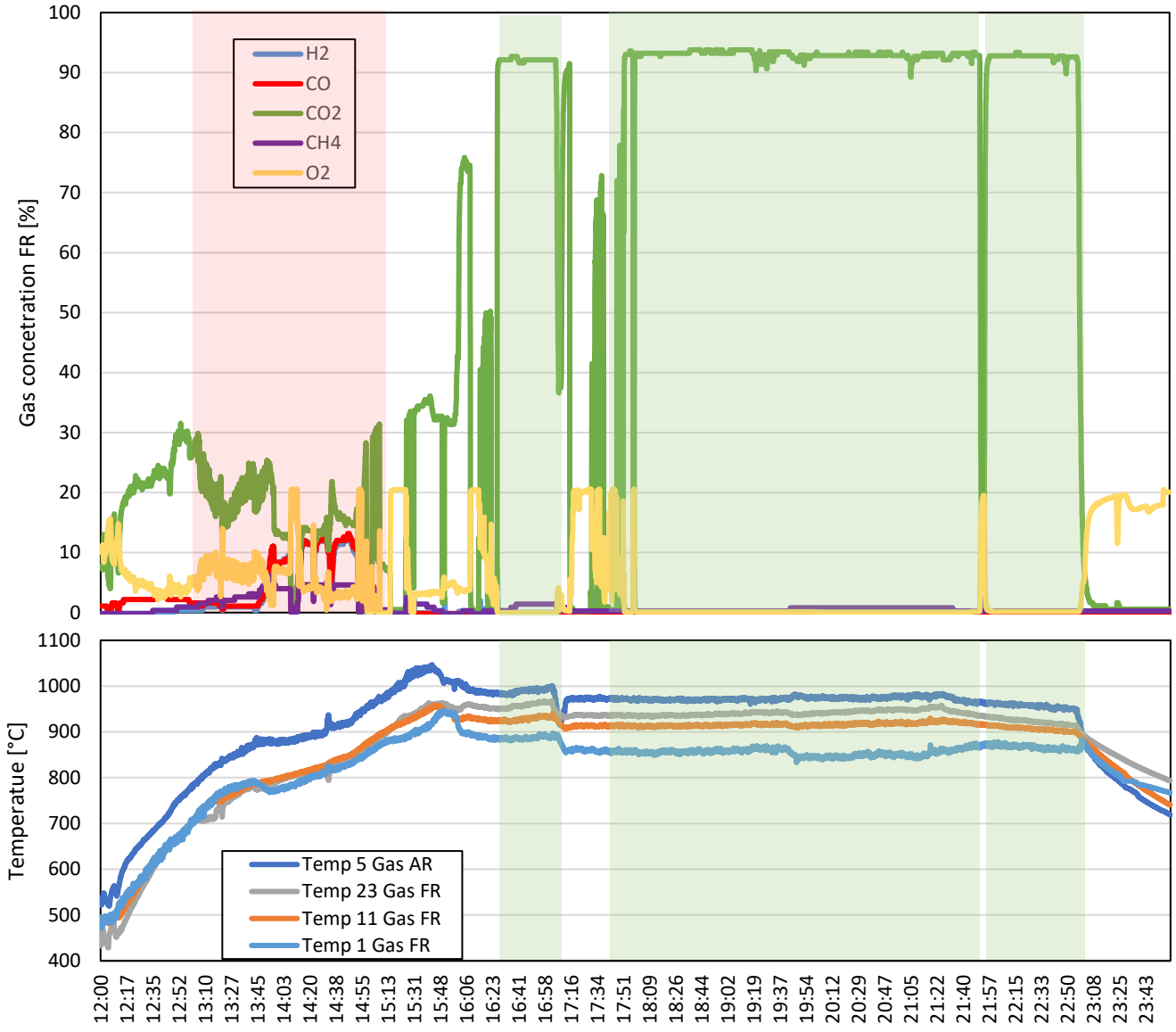

Figure 16: Gas concentration of FR exhaust and temperatures over the duration of the experiment 2 day one with Lana as OC.

triggered a slight decrease in temperature. The CO_2 concentration was high at approximately 93%, whereby the other unburnt components CH_4, CO, H_2 were always below 1.5 %. The concentration of CO and H_2 were below the detection range of the gas measurements. The majority of the rest gas was nitrogen, which was used for flushing of pressure measurements and fuel bunkers. With bark pellets, three steady state operating point were carried with different air staging resulting in variation of the solid circulation rate.

2.2.5 Stationary operating points of experiment 2, solid circulation variation

To investigate the impact of solid circulation rate SCR, there were three different operating points conducted, see Table 12. By shifting the air from tertiary to primary air, SCR could be increased and vice versa. Lana_1.1 showed medium, Lana_1.2 the lowest and Lana_1.3 the highest SCR, which is consistent with the air staging. It should be noted that for Lana_1.3, the fuel rate had to be slightly reduced to prevent the column from flooding. The difference between the oxidation states X_S of the OC of the upper loop seal ULS and lower loop seal increased with lower SCR. That means the OC had to transport more oxygen per kg OC and this could impact stability of the particle in long-term operation. Due to the higher residence time, the oxygen carrier is widely oxidized at low SCR. Lana_1.3 did not showed that trend because of lower amount of fuel.

Table 12: Three OP of the Lana experiments with different SCR, controlled via air staging.

	V_AR_prim [Nm³/h]	V_AR_sec [Nm³/h]	V_AR_tert [Nm³/h]	Add_air [Nm³/h]	V_AR_sum [nm³/h]	**SCR [kg/h]**	X_{S_ULS} [%]	X_{S_LLS} [%]
Lana_1.1	14.1	16.0	21.6	4.0	46.1	**1101.8**	70.6	55.6
Lana_1.2	11.0	15.6	27.7	4.0	49.3	**900.8**	79.0	52.3
Lana_1.3	20.0	16.7	17.7	4.0	50.9	**1285.1**	75.6	65.5

The effect of the solid circulation rate on operation was very clear. With high solid circulation rate the conversion to CO_2 and of other gases was promoted, see Figure 17. The concentration of CO, CH_4, higher hydro-carbons and tars was reduced with higher solid circulation rate. The carbon capture rate seems in contrast to be affected negatively by higher solid circulation rate, showed via Lana_1.3. The carbon capture rate of Lana_1.1 don't support this assumption, whereby the calculated value is mainly based on a concentration measurement of CO_2 of the AR exhaust gas which could have shown a lower accuracy because of the large amount of air. In principle, however, a higher solid circulation rate means a lower residence time of OC particles in the FR. Unburnt fuel and char are carried along with the OC and therefore reduce the carbon capture rate of the process.

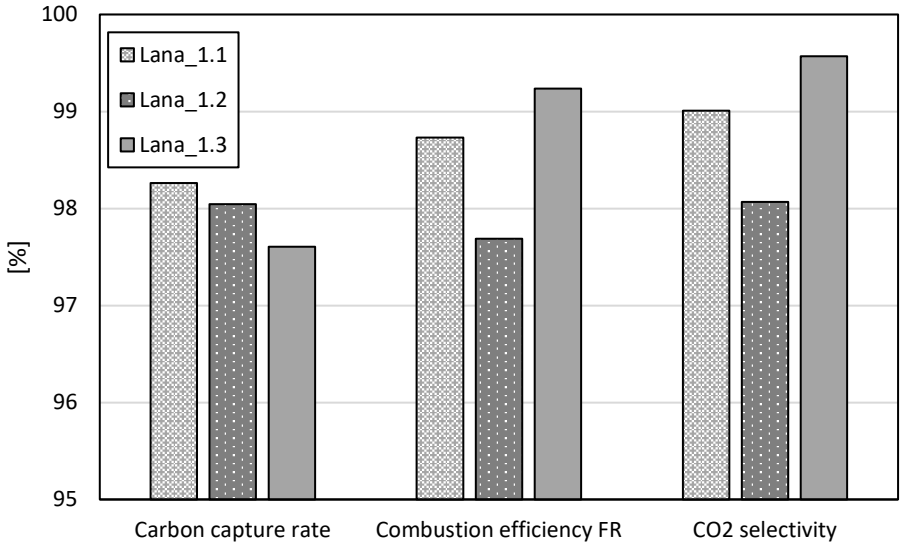

Figure 17: Performance parameters of the three OP comparing impact of solid circulation rate.

Figure 18 shows additional information about the experiments. The Air to fuel ratio and OC to fuel ratio are parameters to better compare the different operating points. Lana_1.3 has the highest values because of higher solid circulation rate and lower amount of fuel. The air to fuel ratio of Lana_1.1 is slightly lower because of the different total volume flow of air. The total oxygen demand indicates the quality of the combustion and how much addition oxygen would be necessary for full combustion. Lana_1.3 would have needed in addition below 1% of the stoichiometric oxygen for full combustion.

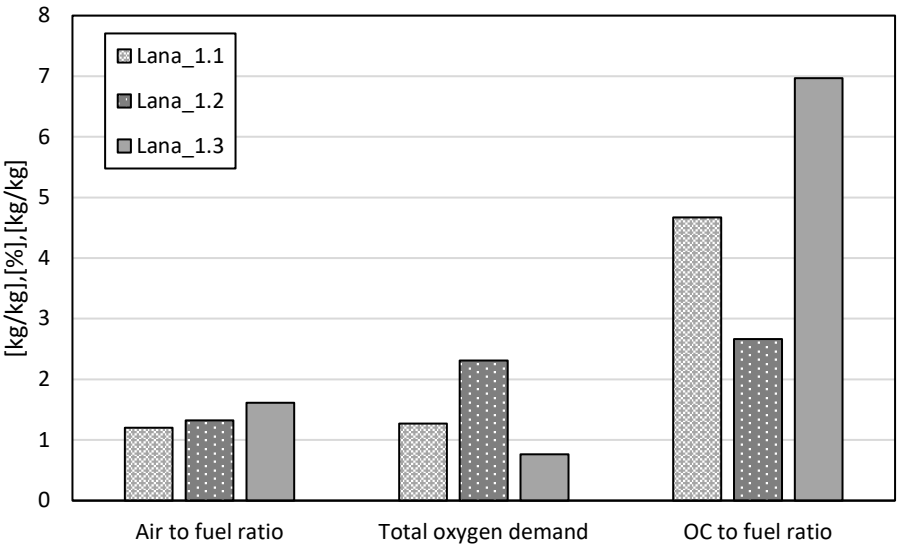

Figure 18: Addition parameters of the three OP comparing solid circulation rates.

2.2.6 Experiment 2 day 2, counter current Column

On experimental day two with Lana, the gas concentrations of different height were measured in the counter current column. Unfortunately, the amount of dust complicated the measurement. The gas measurements of the different stages were blocked after a short time and in place of

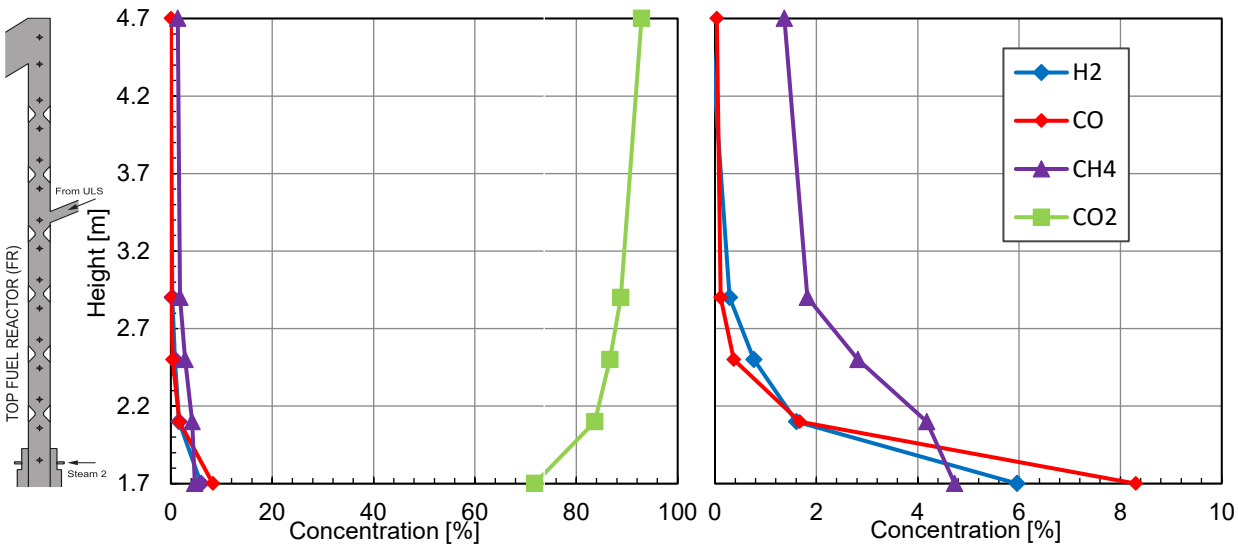

Figure 19: Gas concentration of the counter current column of the FR, experimental day 2 with Lana.

gas from the reactor ambient air was sucked by the pump. This made the bypassing of gas from a height higher than of 3 m not possible. Also, the measurement at 3 m was partly blocked by dust and the measurement was contaminated by air intake. However, since oxygen was also measured, the concentration of the other gases could be obtained mathematically. First of all, the effect of counter current column could be proven, because a concentration increases of CO_2 from 70% to over 90% was measured, see Figure 19. Most of the gas reacts in the area of the first constriction to CO_2. The measurement showed that methane was the most stable component. The hydrogen concentration fell also rather slowly, because the decomposition of methane produces new hydrogen. The measurement of CO was under the detection range of the 5-components measurements device and was in addition measurement with a device in ppm accuracy. The CO concentration was reduced to 355 ppm over the column. In general, it can be said that a very stable operating point was targeted in order to be able to keep it constant for a long time and the condition were not changed for over 5 h. The operation could have been optimized for example by increasing the solid circulation rate to reach higher gas conversion rates, but with that the risk of flooding the column or discharging OC also goes up. This is the reason why the methane concentration was higher than on experimental day 1. For operating point on day 2, an estimation of the height required for full gas conversion could be calculated. A logarithmic approach showed that with a column height of 6 m the methane concentration could be reduced to below 0.5%. The increase of height would have a proportional higher effect with higher solid circulation rates and this experiment was conducted with only moderate circulation rate. The results ultimately proved that the gas conversion can be regulated to a large extent to the chemical equilibrium via the height of the reactor. In the further course of the experiment, the constrictions of the FR were adapted to improve gas/solid contact and gas conversion. In addition to the existing constriction, a tube can be inserted at every constriction to further reduce the area of the counter current column, see Figure 20 the brown tube [34]. The constrictions were narrowed until just before limiting occurred due to flooding of the reactor. While the fifth and sixth constriction were inserted to the half of the reactor, about 6 cm, the other constrictions from first to fourth were only inserted 2 cm. Due to the change in transverse sections, increased accumulation of bed material took place over the narrow area. This led to

an increased gas solid contact and the gas concentration could be influenced. The CO_2 concentration increased by 0.4% to 93.1%, while the CO concentration decreased by 100 ppm. A change of the methane concentration was outside the detection range of the measurement device. When comparing the effects of the constrictions and increasement of SCR, both proved to be beneficial for gas conversion by creating a dense spot of bed material. However, the impact of the solid circulation is higher, because the oxygen and heat transport are also increased. Constriction and circulation, both of are very much limited by flooding of the counter current column. So, if flooding is the main limiting factor, it is always better to increase solid circulation rate. However, when SCR cannot be increased due to other reasons, the expansion of the constrictions is a viable way of increasing operation efficiency.

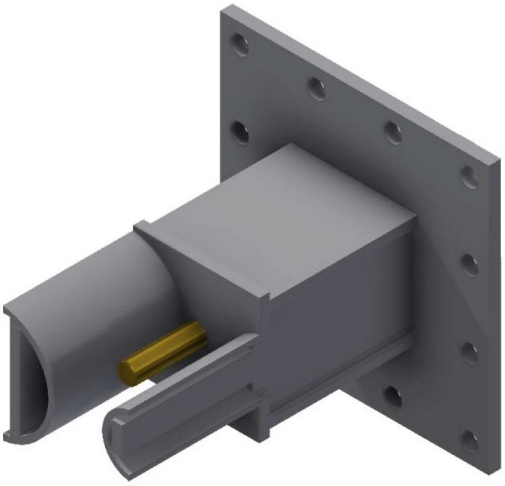

Figure 20: Constrictions with adjustable tube to further decrease the cross section of the counter current column.

2.2.7 Solid sampling

At most stationary operating points, solid samples were taken. With high dust and concentration of fines the extraction was hindered in some cases. The solid sample was flushed with nitrogen to dry the particle from water and prevent contact with ambient air, see Figure 21. After cooling down, the solid sample was filled from the extraction container to airtight glass bottle while still purging the sample and bottle with nitrogen. The glass bottle was then sealed, ready for transport and for further analysis. Due to extended nitrogen flushing the solid samples were dried and no exicator box was necessary. The solid sample were handed over to the project partners and it was planned to carry out analyses of ash surface, phase formation, char concentration, oxidation state and microscopic surface. In addition to this, part of the OC that is left behind when filling the OC from extraction container to glass bottle and is thus contaminated with air, was immediately evaluated. The oxidation state X_S was calculated by weighing and oxidizing in an oven, oxidize, according to a method of Kolbitsch et al. [6].

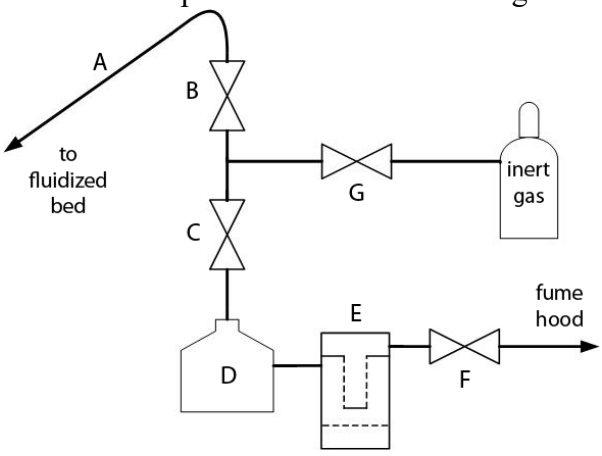

Figure 21: Scheme of the solid sampling procedure, with inert nitrogen flushing.

2.3 Summary project 4

The work in project 1.4 up to milestone 4.1 included two experiments on the 80 kW pilot plant at TU Wien. The base OC ilmenite with limestone and the synthetic OC C28/Lana with wood and bark pellets were used. The first experiment was focused on establishing a baseline experiment, improving ilmenite by mixing it with lime and investigating the influence of temperature change based on autothermal conditions. The results of the first experiments showed indeed an improvement to pure ilmenite. It was also shown that the temperature could only be regulated by oil injection, which highly affected operation. In autothermal operation the temperature adjusted and was depended on other parameters like solid circulation rate, fuel input, steam and air fluidization. It was also shown that the temperature in the FR has an effect on carbon capture rate and decomposition of methane. The second experiment with a synthetic OC was conducted to investigate the influence of the solid circulation rate and the impact of the counter current column. The results showed that the solid circulation rate is a major lever to increase gas conversion, but possible decreasing the carbon capture rate. Another way of increasing the gas conversion is the height of FR and counter current column. With the constriction along the height the CO_2 concentration was increased from 70% to over 90%. In addition, the increase of the constriction area was investigated. However, the application in the experiment was limited due the risk of flooding the column. It showed minor positive effects on gas conversion. Increasing the solid circulation was more effective action to improve gas conversion, because with both actions occur limits by flooding of the column.

Abbreviations

AR	Air reactor
BET	Brunauer Emmett Teller
C28/Lana	Synthetic perovskite oxygen carrier
CLC	Chemical looping combustion
CLOU	Chemical looping with oxygen uncoupling
DFB	Dual fluidized bed
Esam	Euro Support Advanced Materials
FR	Fuel reactor
ILS	Inner loop seal
IPSEPRO	Simulation software
LLS	Lower loop seal
OP	Operating point
Oxy	Oxidation

PSE	Process Simulation Environment
RED	Reduction
RME	Rape methyl ester
SCR	Solid circulation rate
SEM	Scanning electron microscope
TGA	Thermogravimetric analysis
ULS	Upper loop seal
XRD	X-ray diffraction
XRF	X-ray fluorescence

Symbols

Add_air	[m³/h]	Addition air in Air reactor
A_{tot}	[%/h]	Attrition rate
d_{sv}	[µm]	Sauter mean diameter
$m_{f,t}$	[kg]	Mass of fine discharged particles
$m_{O2,st}$	[kg]	Mass of oxygen for stoichiometric combustion
$m_{specific\_FRtop}$	[kg/MW]	Specific bed mass located at top of the FR
$n_{C,CO2,FR,exhaust}$	[mol/s]	mol flow of carbon of FR CO2 exhaust
$n_{C,FR,exhaust}$	[mol/s]	mol flow of carbon of FR exhaust
$n_{C,FR,exhaust}$	[mol/s]	mol flow of carbon of FR exhaust
$n_{C,FR,feed}$	[mol/s]	mol flow of carbon of FR fuel feed
$n_{C,fuel}$	[mol]	mol of carbon in fuel
$n_{C,gas}$	[mol]	mol of carbon in exhaust gas
$n_{C,n}$	[mol]	mol of carbon of gas specie in exhaust gas
$n_{O2,fuel,dem}$	[mol/s]	mol flow of oxygen for combustion of FR fuel feed
$n_{O2exhaust,dem}$	[mol/s]	mol flow of oxygen for combustion of FR exhaust
R_O	[kg/kg]	Oxygen transport capacity
S_n	[%]	Selectivity of certain gas specie
t_{T2-F1}	[h]	Timestamp from Experiment T2 to F1

$V_{\_AR\_prim}$	[nm³/h]	Primary volume flow air reactor
$V_{\_AR\_sec}$	[nm³/h]	Secondary volume flow air reactor
$V_{\_AR\_sum}$	[nm³/h]	Total volume flow air reactor
$V_{\_AR\_tert}$	[nm³/h]	Tertiary volume flow air reactor
X_C	[%]	Carbon conversion
X_{S_LLS}	[%]	Oxidation state lower loop seal
X_{S_ULS}	[%]	Oxidation state upper loop seal
Y_{CO2}	[%]	Yield of CO2
Y_n	[%]	Yield of certain gas specie
ε	[-]	Bed porosity according to REH
η_{CC}	[%]	Carbon capture rate
η_{comb}	[%]	Combustion efficiency
ρ	[kg/m^3]	Density
ρ_b	[kg/m^3]	Bulk density
φ	[kg/kg]	Oxygen of OC to fuel ration
ϕ_i	[%]	Gas concentration
Ω_{OD}	[%]	Oxygen demand for full combustion

Appendix I

This sub-report covers the X-ray Diffraction (XRD)-analysis carried out at TU Wien as part of the BioLoop project. It includes the three different oxygen carrier Ilmenite, Braunite and a manganese ore. For every oxygen carrier there were two XRD- analysis conducted, one before the experiments of Milestone 1.1 and one after that. The goal was first of all to identify the oxide phase and structure of these three natural ores. Moreover, the second XRD-analysis should show if phase change of the material occurred during the experiments. A detailed description of the oxygen carrier and the experiments is given in Milestone 1.1 “Specifications for oxygen carrier (for Chemical Looping Combustion) defined”.

X-ray Diffraction

X-ray diffraction is a powerful non-destructive technique for characterizing crystalline materials. It provides information on structures, phases, preferred crystal orientations. XRD peaks are produced by constructive interference of a monochromatic beam of X-rays scattered at specific angles from each set of lattice planes in a sample. The peak intensities are determined by the atomic positions within the lattice planes. Consequently, the XRD pattern is the fingerprint of periodic atomic arrangements in a given material. An online search of a standard database for X-ray powder diffraction patterns enables quick phase identification for a large variety of crystalline samples. [35]

Ilmenite

Pre-experiment

Fresh Ilmenite consist mainly of a titanium-iron-oxide phase and iron phase. This is also confirmed by the elemental analysis, where high iron and titanium concentration are measured, to be found in Milestone 1.1. There are also some other common impurities that are common for natural ores like quartz, calcium- and silicon oxides. With XRD-analyse, also the approximate fraction of the phase could be determined, but only of the crystalline structure.

Phase	Element formula	Fraction	Addition info
Titanium Iron Oxide	Ti0.79Fe1.2O3	50%	-
Hematite, Ti-bearing	Ti0.14Fe1.86O3	30%	-
Quartz	SiO2	-	-
Calcium Manganese Silicate	Ca0.5Mn0.5SiO3	-	-

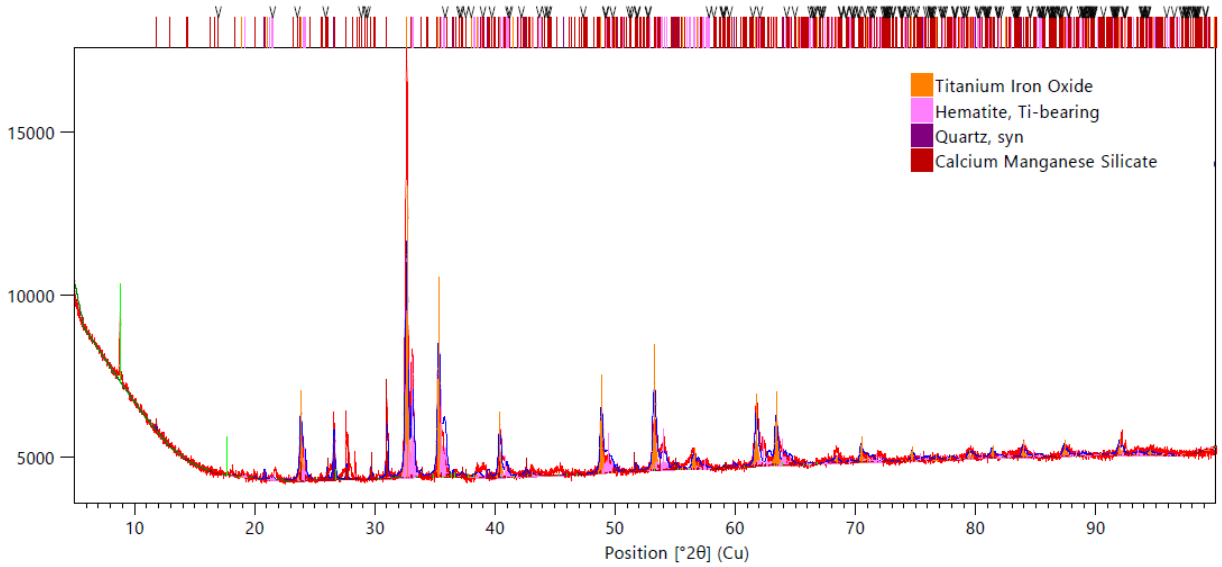

Figure 22: XRD-analysis with fresh Ilmenite.

Post experiment

The Ilmenite was analysed after the experiments again, but the interpretation of the different peaks become difficult. Interference with ash and the building of new phases increased the amount of background noise. Nevertheless, a phase change form Titanium-iron-oxide to Pseudo brookite could identified clearly. This also showed in the appearance of the oxygen carrier, because the Pseudo brookite phase tends to take on a red brown colour. The Pseudo brookite phase is able to extend amount of oxygen, which is stored. An activation, also shown with the experimental results, is the consequence. Furthermore, a crystal structure change to an orthorhombic system took place.

Phase	Element formula	Fraction	Addition info
Pseudo brookite	TiFeO5	55	orthorhombic
Hematite, Ti-bearing	Ti0.14Fe1.86O3	18	-
Titanium Iron Oxide	Ti0.79Fe1.2O3	5	-
Donpeacorite	MgMnSiO6	-	-

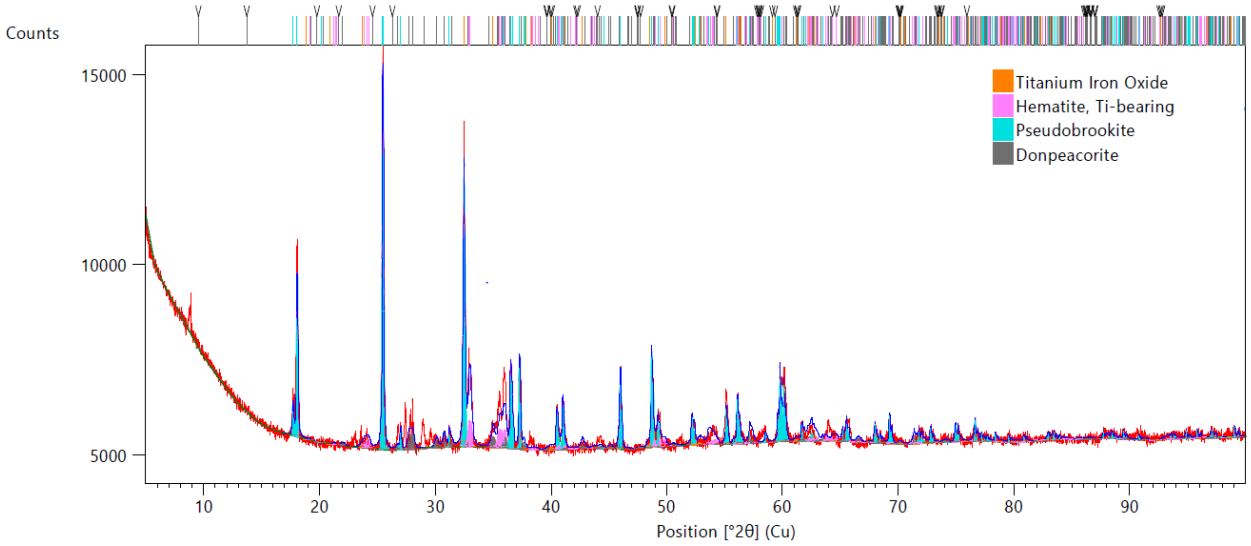

Figure 23: XRD-analysis with used Ilmenite after the experiment.

Braunite

Pre-experiment

Braunite has besides high concentration of manganese oxide, high amounts of impurities. The main other components are iron and silicon. Because of the many different phases with only small fraction of the total metal oxides, the analysis of Braunite was especially challenging. The main phase of Braunite was Braunite-1Q, which is a manganese silicate.

Phase	Element formula	Fraction	Addition info
Braunite-1Q	$Mn_7(SiO_4)O_8$	51	-
Manganese oxide	Mn_2O_3	39	-
Hematite	Fe_2O_3	4	A-rhombic
Rest	-	-	Ca, Al, S, Ca, Fe

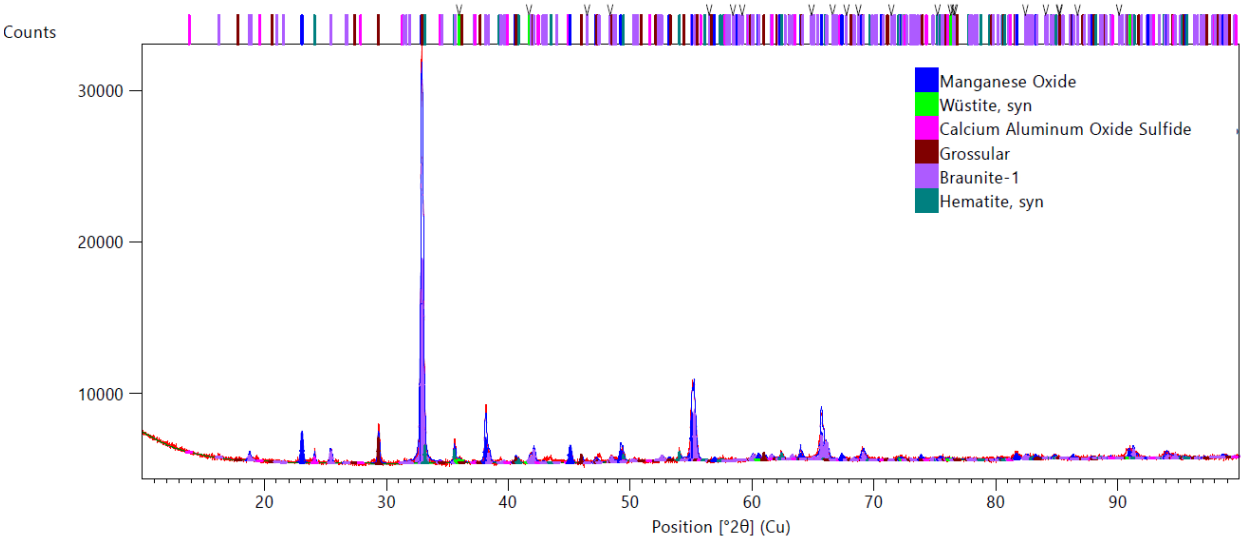

Figure 24: XRD-analysis with fresh Braunite.

Post-experiment

The XRD-analysis showed after the experiments more phases, that were difficult to identify. The phase Braunite-1Q almost completely transformed to Haus mannite. With a lower amount of oxygen stored in this phase, the activation of the Braunite could be explained. Also, reoxidation of the manganese to higher oxidation state would not occur with the given temperatures in the CLC process. This means that the initial oxygen uncoupling effect of Braunite declines over the experimental time. The transformation of the phase Haus mannite to a spinel, tetragonal crystalline structure, could also be reason for the extended attrition of the Braunite.

Phase	Element formula	Fraction	Addition info
Haus mannite	Mn3O4	35	Spinel, tetragonal
Manganese oxide	Mn2O3	29	-
Braunite-1Q	Mn7(SiO4)O8	4	rhombic
Iron oxide	F2O3	-	orthorhombic
Rest	-	-	Ca, Al, S, Ca, Fe

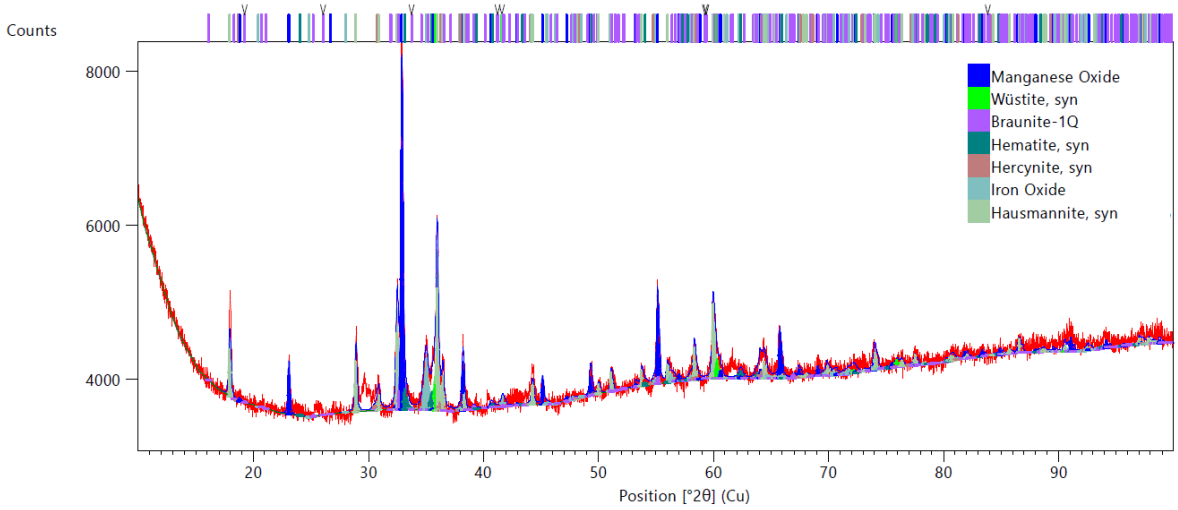

Figure 25: XRD-analysis with used Braunite after the experiment.

Mn ore

Pre-experiment

The composition of the Mn ore mainly consists of manganese, iron and silicon. The fact that the phases are present individually and not as mixed phases like with the Braunite, could be an indicator for the increased reactivity of the Mn ore. In addition, the XRD-analysis, leads to the conclusion that iron concentration could be higher than the elemental analysis showed. An investigation of scanning electron microscope SEM confirms this assumption.

Phase	Element formula	Fraction	Addition info
Hematite	Fe2O3	42	-
Manganese oxide	Mn2O3	30	-
Silicon oxide	SiO2	-	-
Jacobsite	Mn0.9Fe2O4	-	-

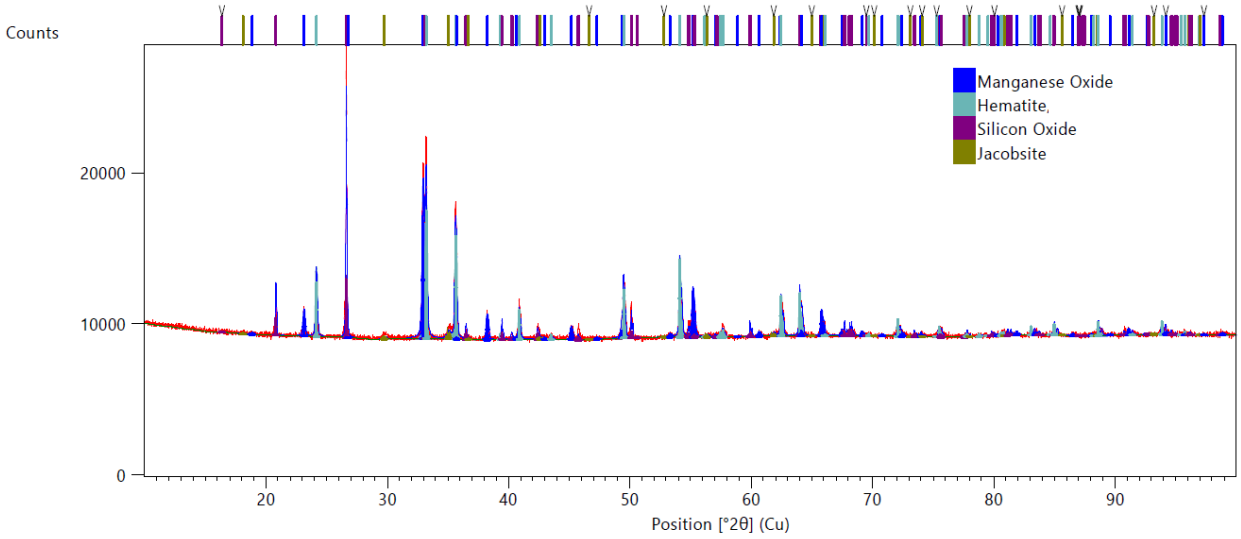

Figure 26: XRD-analysis with fresh Mn ore.

Post-experiment

After the experiments, a phase transformation to Jacobsite is visible. The amount of Hematite and Manganese oxide decreased, but no new phases were discovered. Jacobsite can store less oxygen than the other phases. This implies a deactivation of the Mn ore over the experimental time. In addition, the oxygen release decreased from first to fifth experiment.

Phase	Element formula	Fraction	Addition info
Hematite	Fe2O3	40	-
Jacobsite	Mn0.9Fe2O4	34	-
Manganese oxide	Mn2O3	7	-
Silicon oxide	SiO2	-	-

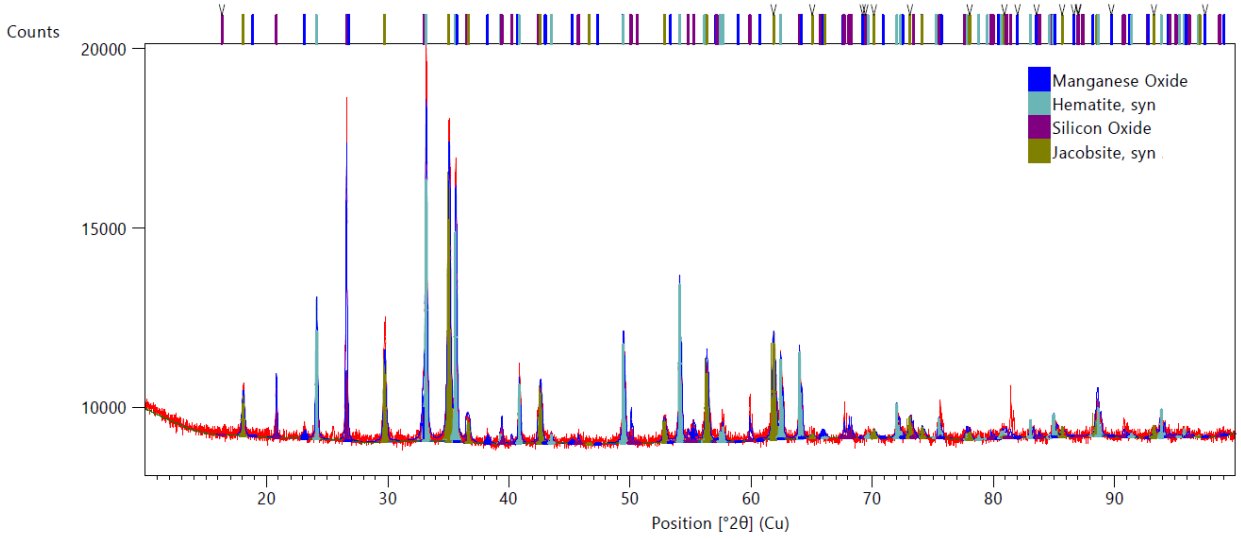

Figure 27: XRD-analysis with used Mn Ore after the experiment.

Summary XRD

The XRD-analysis of the experiments was successful identifying the main phases and phase transformation of the natural ores. Minor impurities or the impact of ash on the structure could not be found. The activation and deactivation of the three oxygen carries, which happened during the experiments, could be confirmed by identifying phase transformation. The manganese containing ores transformed to state with less oxygen transport capacity and possible less amount of oxygen uncouples. The Pseudo brookite phase of the Ilmenite expand, which proved to be an improvement of structure, reactivity and oxygen transport.

Appendix II

This sub-report covers the Scanning electron microscope (SEM) and Brunauer–Emmett–Teller (BET) analysis carried out at TU Wien as part of the BioLoop project. It includes the three different oxygen carrier Ilmenite, Braunite and a manganese ore. Every oxygen carrier was investigated, before the experiments of Milestone 1.1 and after that. The goal was to identify the changes in structure, surface and reactivity over the duration of the experiments. A detailed description of the oxygen carrier and the experiments is given in Milestone 1.1 “Specifications for oxygen carrier (for Chemical Looping Combustion) defined”.

Methods

SEM

The scanning electron microscope (SEM) is electron microscope that uses a focused beam of electrons to produces images of a sample by scanning the surface with a. The electrons interact with atoms in the sample, producing various signals that contain information about the surface topography and composition of the sample. Accelerated electrons in an SEM carry significant amounts of kinetic energy, and this energy is dissipated as a variety of signals produced by electron-sample interactions when the incident electrons are decelerated in the solid sample. Secondary electrons and backscattered electrons are commonly used for imaging samples: secondary electrons are most valuable for showing morphology and topography on samples and backscattered electrons are most valuable for illustrating contrasts in composition in multiphase samples.

BET

In BET surface area analysis, nitrogen is usually used because of its availability in high purity and its strong interaction with most solids. Because the interaction between gaseous and solid phases is usually weak, the surface is cooled using liquid N_2 to obtain detectable amounts of adsorption. Known amounts of nitrogen gas are then released stepwise into the sample cell. Relative pressures less than atmospheric pressure are achieved by creating conditions of partial vacuum. After the saturation pressure, no more adsorption occurs regardless of any further increase in pressure. After the adsorption layers are formed, the sample is removed from the nitrogen atmosphere and heated to cause the adsorbed nitrogen to be released from the material and quantified. The data collected is displayed in the form of a BET isotherm, which plots the amount of gas adsorbed as a function of the relative pressure.

Results

SEM Ilmenite

Before: After:

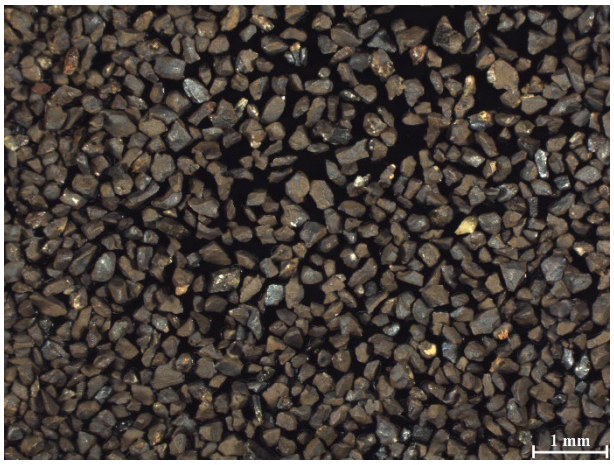

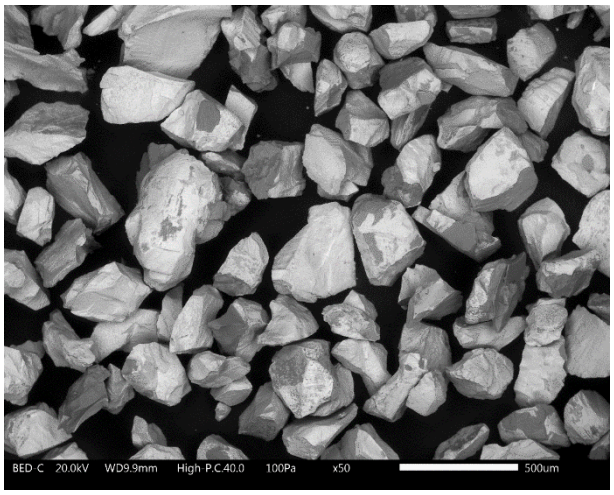

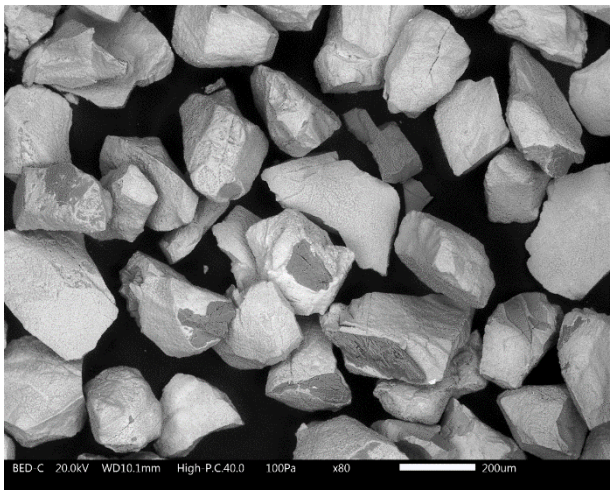

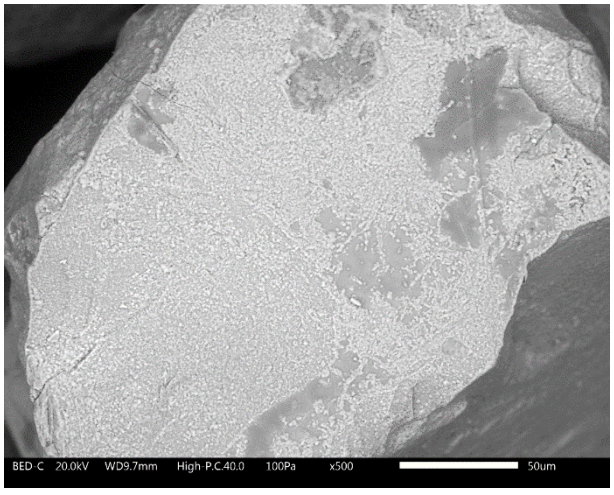

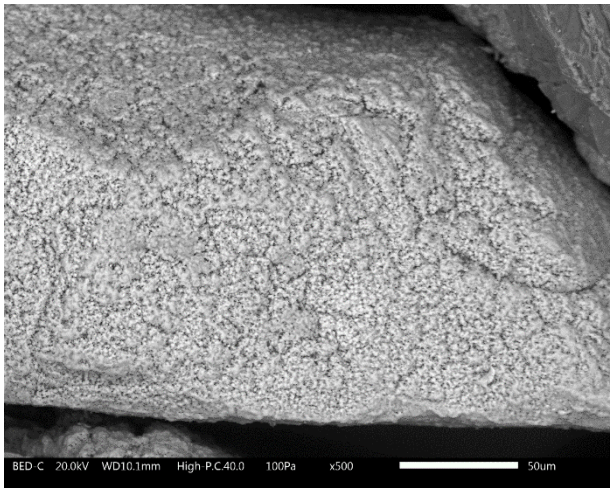

The SEM analysis shows a fundamental structural change of the ilmenite particles, which can also be recognized by a colour change. At medium resolution, a rounding of the sharp edges of the particles and increased iron phase formation on the surface of the particle can be seen. The

50 micrometre solution shows a strong surface change from smooth to more porous structures, which also explains the increase in reactivity of ilmenite over the experiment.

SEM Braunite

Before:

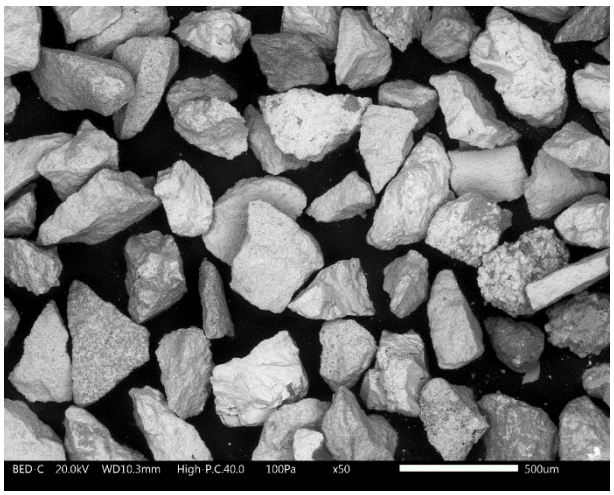

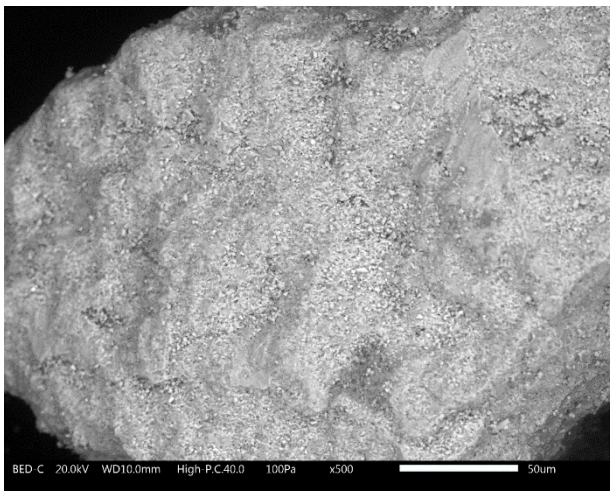

After:

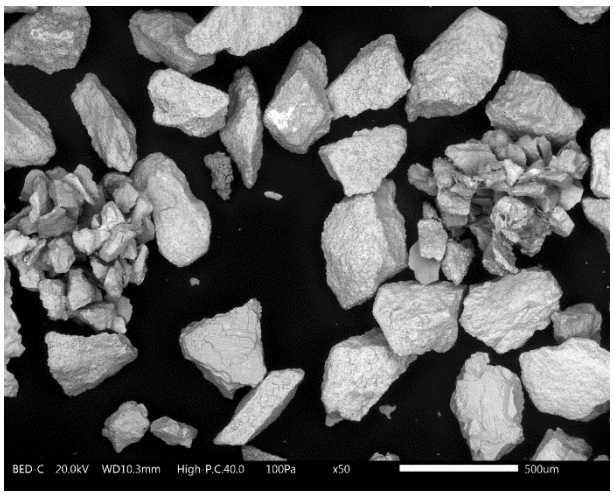

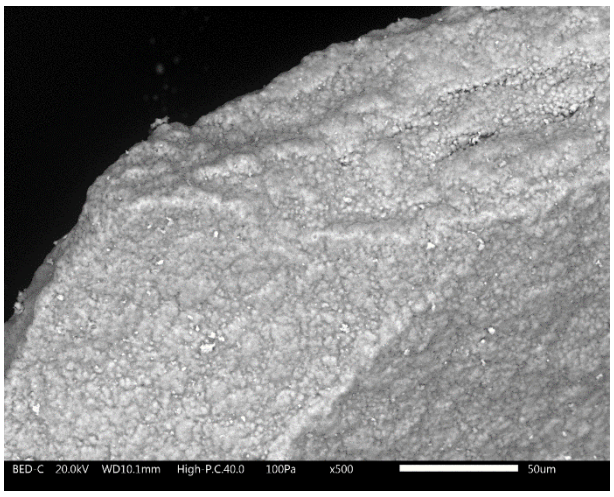

The Sem analysis of the Braunite particles shows a reduction in average particle size triggered by attrition. However, individual particles also form particle agglomerates, which almost compensate for the effect on particle size distribution. The analysis of the surface shows very

porous structures before the experiment. These seem to be abraded by the experiment. Instead, cracks can be seen, which indicate the beginning of abrasion or particle breakage.

SEM Mn ore

Before: After:

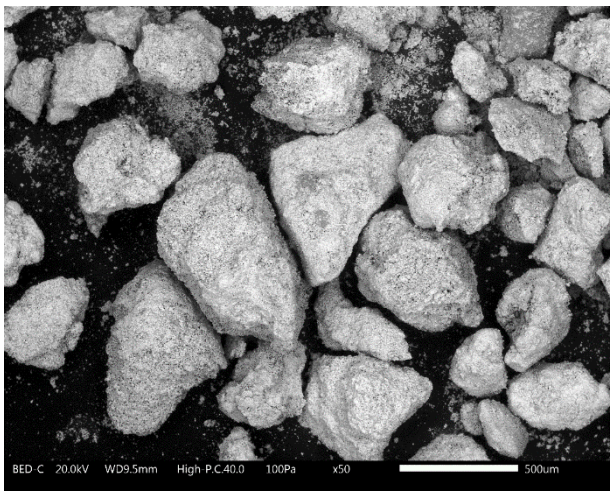

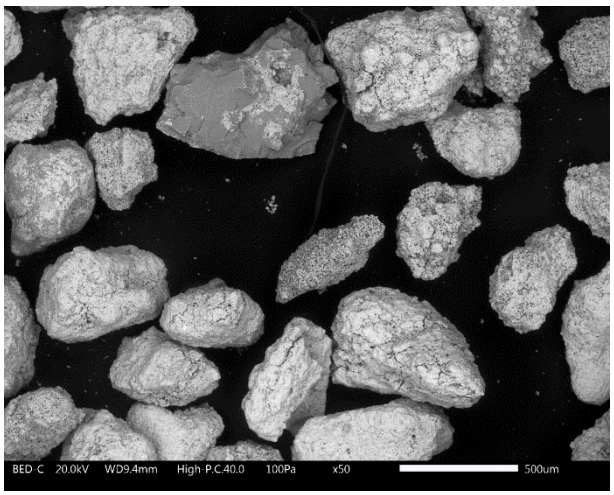

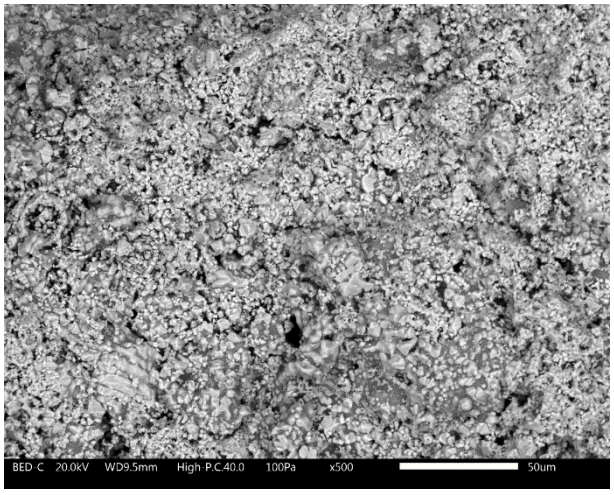

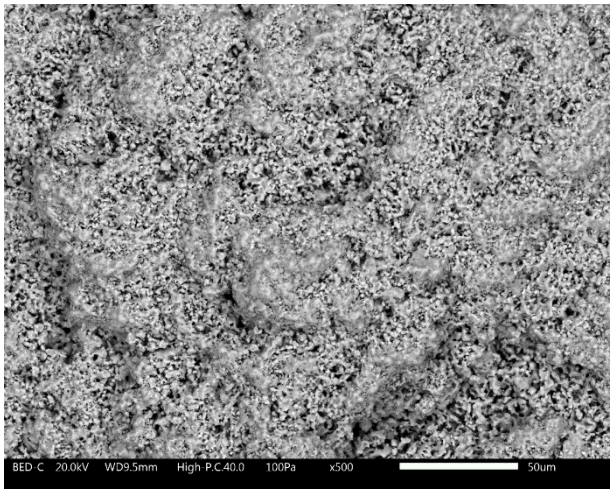

SEM analysis of Mn ore shows mainly large amounts of fines. In the images taken after the experiment, this fraction is reduced by the discharge of the fine particles. The particle surface

is characterized by uneven porous structures, which are also preserved over the experimental time.

BET

The isotherms of the materials could be recorded via the uptake and release of nitrogen under the influence of different pressures. This is shown by the example of Mn ore before the experiment, see Figure 1.

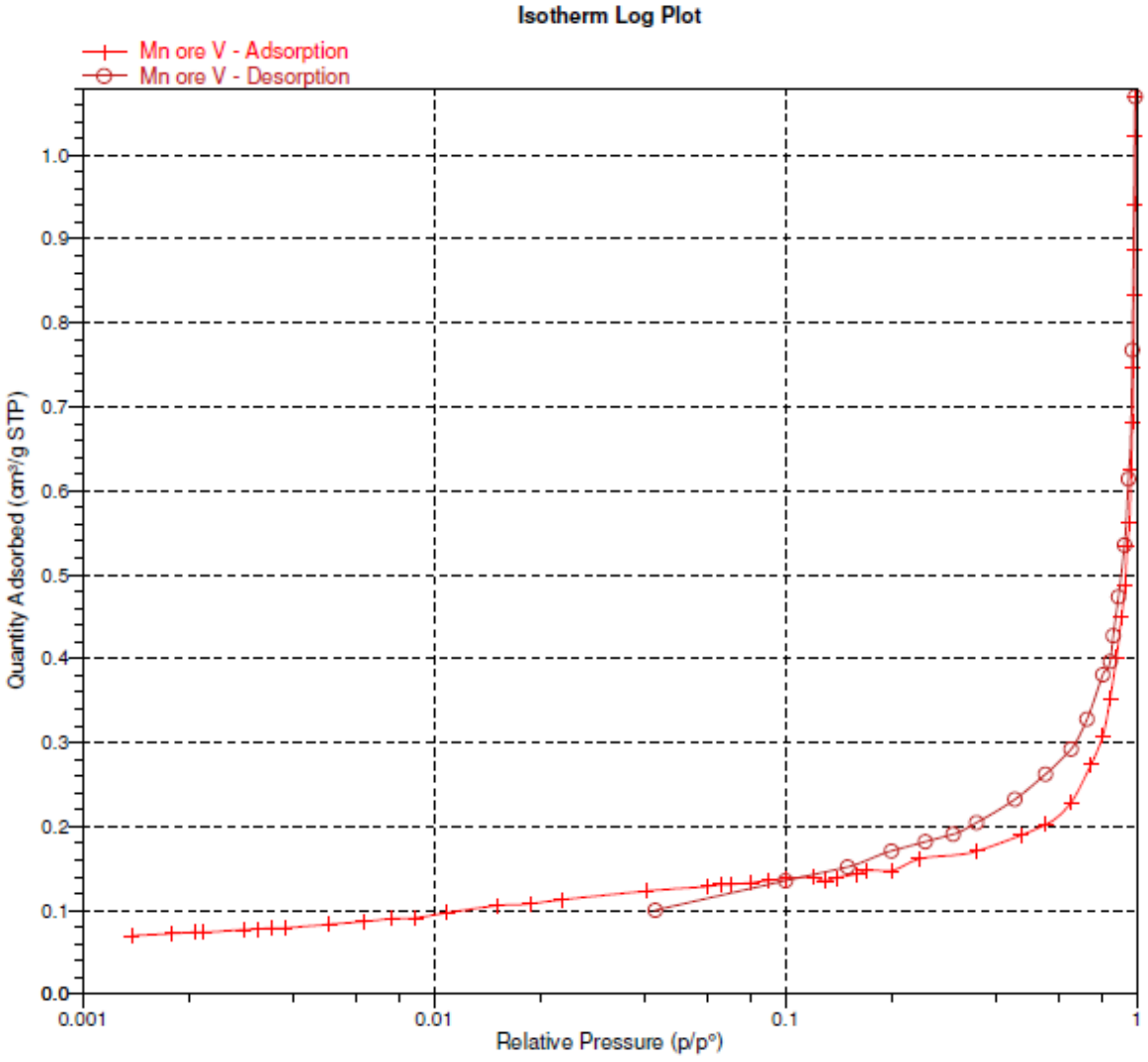

Figure 28: Isotherm Log Plot of Mn ore before the experiment.

The BET analysis of ilmenite was in the very low range, and was almost below the detection limit of the method. This also explains a lower reactivity than the other ores. A surface increase, which can be seen in the SEM images, could not be detected in the ilmenite. This may also be due to the accuracy of the instrument in the low detection range. The surface area of the two manganese-bearing ores is approximately the same for the fresh samples. Braunite shows as already indicated in the SEM analysis a dramatic reduction of the surface. Mn ore shows a small increase, see Figure 2.

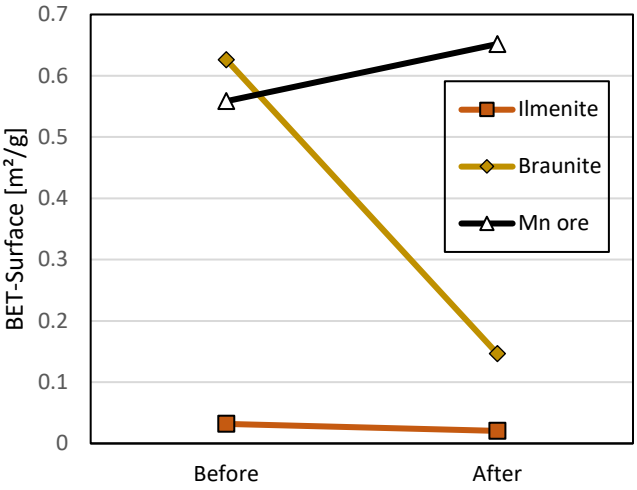

Figure 29: BET-Surface of the three ores before and after the experiments.

Summary SEM/BET

The performed analyses could basically confirm some assumptions based on the experiment. Ilmenite underwent a phase change leading to an increase in reactivity and a more porous surface. This could not be confirmed by BET due to the low resolution. Braunite showed increased abrasion and decreasing reactivity, affected by lower surface area after the experiment. In the case of Mn ore, a reduction of the fine fraction was observed. This, however, did not lead to a reduction of the reactive surface of the particles, but nevertheless to a reduction of the conversion over the experiment. The reason may be the overall reduction of the bed material mass due to the addition of the fines. In any case, the present analyses cannot replace the experimental investigation of the oxygen carriers and can only act complementary to the knowledge generation.

Literature

[1] R. Pachler, Chemical looping combustion – a sustainable combustion technology for negative emission energy production, in, TU Vienna, Vienna, 2019.
[2] B. Fleiß, J. Fuchs, S. Penthor, S. Arlt, R. Pachler, S. Müller, H. Hofbauer, Innovative laboratory unit for pre-testing of oxygen carriers for chemical-looping combustion, Biomass Conversion and Biorefinery, (2021).
[3] K. Mayer, S. Piesenberger, S. Penthor, T. Pröll, H. Hofbauer, Chemical Looping Combustion Using Two Different Perovskite Based Oxygen Carriers: A Pilot Study, Energy Technology, (2018).
[4] J. Adánez, L.F. de Diego, F. García-Labiano, P. Gayán, A. Abad, J.M. Palacios, Selection of Oxygen Carriers for Chemical-Looping Combustion, Energy & Fuels, 18 (2004) 371-377.
[5] F. Benedikt, J. Fuchs, J.C. Schmid, S. Müller, H. Hofbauer, Advanced dual fluidized bed steam gasification of wood and lignite with calcite as bed material, Korean Journal of Chemical Engineering, 34 (2017) 2548-2558.
[6] P. Kolbitsch, T. Pröll, J. Bolhar-Nordenkampf, H. Hofbauer, Characterization of Chemical Looping Pilot Plant Performance via Experimental Determination of Solids Conversion, Energy & Fuels, 23 (2009) 1450-1455.

[7] M. Rydén, P. Moldenhauer, S. Lindqvist, T. Mattisson, A. Lyngfelt, Measuring attrition resistance of oxygen carrier particles for chemical looping combustion with a customized jet cup, Powder Technology, 256 (2014) 75-86.
[8] D. Mei, H. Zhao, Z. Ma, C. Zheng, Using the Sol–Gel-Derived CuO/CuAl2O4 Oxygen Carrier in Chemical Looping with Oxygen Uncoupling for Three Typical Coals, Energy & Fuels, 27 (2013) 2723-2731.
[9] L.P.R. Pala, Q. Wang, G. Kolb, V. Hessel, Steam gasification of biomass with subsequent syngas adjustment using shift reaction for syngas production: An Aspen Plus model, Renewable Energy, 101 (2017) 484-492.
[10] R. Solimene, A. Marzocchella, P. Salatino, Hydrodynamic interaction between a coarse gas-emitting particle and a gas fluidized bed of finer solids, Powder Technology, 133 (2003) 79-90.
[11] J. Schmid, T. Pröll, C. Pfeifer, R. Rauch, H. Hofbauer, Cold Flow Model Investigation on a Modified Riser with Enhanced Gas-Solid Contact: Locating the Regions of Operation in a Fluidization Regime Map, in: 21st International Conference on Fluidized Bed Combustion (FBC), Naples, Italy, 2012.
[12] J.M. Fan, H. Hong, H.G. Jin, Life cycle global warming impact of CO2 capture by in-situ gasification chemical looping combustion using ilmenite oxygen carriers, J Clean Prod, 234 (2019) 568-578.
[13] A. Cuadrat, A. Abad, J. Adánez, L.F. de Diego, F. García-Labiano, P. Gayán, Behavior of ilmenite as oxygen carrier in chemical-looping combustion, Fuel Processing Technology, 94 (2012) 101-112.
[14] T. Mendiara, F. García-Labiano, A. Abad, D. Knittler, J.Y. Kim, N. Ellis, Air jet attrition measurements at hot conditions of oxygen carriers for chemical looping combustion, Powder Technology, 392 (2021) 661-671.
[15] G. Tardos, R. Pfeffer, Chemical reaction induced agglomeration and defluidization of fluidized beds, Powder Technology, 85 (1995) 29-35.
[16] M. Matzen, J. Pinkerton, X. Wang, Y. Demirel, Use of natural ores as oxygen carriers in chemical looping combustion: A review, International Journal of Greenhouse Gas Control, 65 (2017) 1-14.
[17] D. Mei, C. Linderholm, A. Lyngfelt, Performance of an oxy-polishing step in the 100 kWth chemical looping combustion prototype, Chemical Engineering Journal, 409 (2021).
[18] I. Adánez-Rubio, H. Bautista, M.T. Izquierdo, P. Gayán, A. Abad, J. Adánez, Development of a magnetic Cu-based oxygen carrier for the chemical looping with oxygen uncoupling (CLOU) process, Fuel Processing Technology, 218 (2021).
[19] P. Markström, C. Linderholm, A. Lyngfelt, Chemical-looping combustion of solid fuels – Design and operation of a 100kW unit with bituminous coal, International Journal of Greenhouse Gas Control, 15 (2013) 150-162.
[20] A. Abad, I. Adánez-Rubio, P. Gayán, F. García-Labiano, L.F. de Diego, J. Adánez, Demonstration of chemical-looping with oxygen uncoupling (CLOU) process in a 1.5kWth continuously operating unit using a Cu-based oxygen-carrier, International Journal of Greenhouse Gas Control, 6 (2012) 189-200.
[21] T. Pröll, H. Hofbauer, A dual fluidized bed system for chemical looping combustion of solid fuels, Proceedings of the AIChE Annual Meeting 2010 Salt Lake City, USA, (2010).
[22] J. Schmid, T. Pröll, C. Pfeifer, H. Hofbauer, Improvement of gas-solid interaction in dual circulating fluidized bed systems, in: Proceedings of the 9th Conference on Industrial Furnances and Boilers (INFUB-9) Estoril, Portugal, 2011.
[23] S. Penthor, M. Stollhof, T. Pröll, H. Hofbauer, Detailed fluid dynamic investigations of a novel fuel reactor concept for chemical looping combustion of solid fuels, Powder Technology, 287 (2016) 61-69.
[24] J.C. Schmid, S. Müller, H. Hofbauer, First scientific results with the novel dual fluidized bed gasification test facility at TU Wien, in: 24th European Biomass Conference and Exhibition (EUBCE), ETA-Florence Renewable Energies, Amsterdam, The Netherlands, 2016, pp. 842-846.
[25] J. Fuchs, J. Schmid, S. Müller, H. Hofbauer, Sorption Enhanced Reforming: Transport Characteristics of CO2 and Char, in: 11th International Conference on Sustainable Energy & Environmental Protection, University of the West of Scotland, Paisley, United Kingdom, 2018.
[26] A.M. Mauerhofer, F. Benedikt, J.C. Schmid, J. Fuchs, S. Müller, H. Hofbauer, Influence of different bed material mixtures on dual fluidized bed steam gasification, Energy, 157 (2018) 957-968.

[27] S. Müller, J. Fuchs, J.C. Schmid, F. Benedikt, H. Hofbauer, Experimental development of sorption enhanced reforming by the use of an advanced gasification test plant, International Journal of Hydrogen Energy, 42 (2017) 29694-29707.
[28] S. Penthor, J. Fuchs, F. Benedikt, J. Schmid, A. Mauerhofer, K. Mayer, H. Hofbauer, First results from an 80 kW dual fluidized bed pilot unit for solid fuels at TU Wien, in: 5th International Conference on Chemical Looping, Park City, Utah, USA, 2018.
[29] B. Fleiß, S. Penthor, S. Müller, H. Hofbauer, J. Fuchs, Holistic assessment of oxygen carriers for chemical looping combustion based on laboratory experiments and validation in 80 kW pilot plant, Fuel Processing Technology, 231 (2022).
[30] T. Mattisson, J. Adánez, K. Mayer, F. Snijkers, G. Williams, E. Wesker, O. Bertsch, A. Lyngfelt, Innovative Oxygen Carriers Uplifting Chemical-looping Combustion, Enrgy Proced, 63 (2014) 113-130.
[31] G. Teyssié, H. Leion, G.L. Schwebel, A. Lyngfelt, T. Mattisson, Influence of Lime Addition to Ilmenite in Chemical-Looping Combustion (CLC) with Solid Fuels, Energy & Fuels, 25 (2011) 3843-3853.
[32] A. Cuadrat, C. Linderholm, A. Abad, A. Lyngfelt, J. Adánez, Influence of Limestone Addition in a 10 kWth Chemical-Looping Combustion Unit Operated with Petcoke, Energy & Fuels, 25 (2011) 4818-4828.
[33] I. Gogolev, A.H. Soleimanisalim, C. Linderholm, A. Lyngfelt, Commissioning, performance benchmarking, and investigation of alkali emissions in a 10 kWth solid fuel chemical looping combustion pilot, Fuel, 287 (2021).
[34] R. Diem, Design, Construction and Startup of an Advanced 100 kW Dual Fluidized Bed System for Thermal Gasification, in, TU Vienna, 2015.
[35] R. Kohli, K.L. Mittal, Chapter 3 - Methods for Assessing Surface Cleanlines, in: Developments in Surface Contamination and Cleaning, Elsevier, 2019.